

1998-05

Neural Dynamics of Binocular Brightness Perception

<https://hdl.handle.net/2144/2353>

"Downloaded from OpenBU. Boston University's institutional repository."

Neural dynamics of binocular brightness perception

Stephen Grossberg and Frank Kelly

April, 1998

Technical Report CAS/CNS-1998-019

Permission to copy without fee all or part of this material is granted provided that: 1. The copies are not made or distributed for direct commercial advantage; 2. the report title, author, document number, and release date appear, and notice is given that copying is by permission of the BOSTON UNIVERSITY CENTER FOR ADAPTIVE SYSTEMS AND DEPARTMENT OF COGNITIVE AND NEURAL SYSTEMS. To copy otherwise, or to republish, requires a fee and / or special permission.

Copyright © 1998

Boston University Center for Adaptive Systems
and
Department of Cognitive and Neural Systems
677 Beacon Street
Boston, MA 02215

NEURAL DYNAMICS OF BINOCULAR BRIGHTNESS PERCEPTION

Stephen Grossberg†

Frank Kelly†

Department of Cognitive and Neural Systems
and Center for Adaptive Systems
Boston University

Submitted: April, 1998

Revised: April, 1999

Technical Report CAS/CNS TR-98-019

All correspondence should be addressed to:

Professor Stephen Grossberg
Department of Cognitive and Neural Systems*
Boston University
677 Beacon Street
Boston, MA 02215
Phone: 617-353-7858
Fax: 617-353-7755
E-mail: steve@bu.edu

Key words: Brightness perception, Binocular vision, Fechner's Paradox,
Ganzfeld, Neural networks, FACADE theory, BCS, FCS

Running Head: Binocular Brightness Summation

† Supported in part by the Defense Advanced Research Projects Agency and the Office of Naval Research (ONR N00014-95-1-0409) and by the Office of Naval Research (ONR N00014-95-1-0657).

‡ The authors wish to thank C. Bourassa for providing the data from his ganzfeld experiments.

*Acknowledgments: The author wishes to thank Diana Meyers for her valuable assistance in the preparation of this manuscript.

Abstract

How does the visual cortex combine information from both eyes to generate perceptual representations of object surfaces? Important clues about this process may be derived from data about the perceived brightnesses of surface regions under binocular viewing conditions, including data about binocular brightness summation in response to ganzfelds, the U-shaped data of Fechner's Paradox that violates binocular brightness summation, and the effects of different combinations of monocular and binocular contours and surface luminance differences on threshold sensitivity to monocular flashes of light. How to reconcile these apparently contradictory data properties has been a severe challenge to previous models, and none has explained them all. The present article quantitatively simulates them all by further developing the FACADE vision model. Key model processes discount the illuminant and compute image contrasts in each monocular channel using shunting on-center off-surround networks; binocularly fuse these discounted monocular signals using shunting on-center off-surround networks with nonlinear excitatory and inhibitory signals; and use these binocularly fused activities to trigger filling-in of a binocular surface representation that represents perceived surface brightness. Previous models that have suggested explanations of subsets of these data are discussed.

1. Introduction

Surfaces dominate our perceptions of the three-dimensional world, yet there are few theoretical explanations of how surfaces acquire their vivid perceptual qualities. As a result, although phenomena of surface brightness and lightness perception have long been experimentally investigated, their meaning and explanation remain an area of intense debate (Gilchrist, 1994). Understanding the neural mechanisms that underlie brightness perception also remains a matter of controversy and continuing research (Arrington, 1994; Paradiso and Nakayama, 1991). Several modeling papers have described different ways in which lightness and brightness perceptions can arise (Gove, Grossberg and Mingolla, 1995; Grossberg and Todorović, 1988; Grossberg and Wyse, 1991; Hamada, 1984; Kingdom and Moulden, 1992; Land and McCann, 1971; see Pessoa, Mingolla and Neumann, 1995 for a review). However most of these perceptual and modeling investigations have looked at 2-D brightness and lightness phenomena; e.g., simultaneous contrast and Mach bands. Recently a line of research has extended the domain into 3-D brightness perception as part of a neural theory of 3-D vision and figure-ground separation, called FACADE theory (Grossberg, 1987, 1994, 1997).

FACADE is an acronym for Form-And-Color-And-DEpth, referring to the multiplexed representations of form and color and depth which the model generates. Recent simulations of FACADE theory have shown how the network can explain challenging data about stereopsis, including dichoptic masking and contrast-dependent variations of Panum's limiting case (McLoughlin and Grossberg, 1998), and da Vinci stereopsis (Grossberg and McLoughlin, 1997). FACADE theory has also offered explanations of lightness illusions, such as the White effect (White, 1979), and of how depthful surface brightness capture occurs during figure-ground separation (Grossberg, 1997; Kelly and Grossberg, 1997). Here we analyze how the visual cortex combines monocular brightness signals to determine binocular brightness percepts as part of the process whereby surface representations are formed.

In this regard, it is well known that the visual system can use the slight disparities introduced by binocular viewing to compute relative distance to an object (Panum, 1858; Wheatstone, 1838). Binocular viewing also provides some other advantages over monocular viewing: binocular improvement occurs for tasks such as detection of stationary targets, luminance flashes and discrimination tasks (see Blake and Fox (1973), Blake, Sloane and Fox (1981) and Howard and Rogers (1995, Chapter 8) for reviews). One might therefore expect that binocular summation occurs during brightness perception, in particular that an illuminated area appears twice as bright if viewed with two eyes than when viewed with one eye. The reader can

easily falsify this supposition by closing one eye and noting that the world does not become half as bright. An illuminated area appears only slightly brighter when viewed with two eyes.

In fact, Panum, and then Fechner, discovered that a bright light presented to one eye may actually appear less bright when a dim light is shone into the other eye, in what has since become known as *Fechner's Paradox* (Aubert, 1865; Fechner, 1861; Panum, 1858). The effect is paradoxical since, despite the increased total stimulation on both retinas, the perceived binocular brightness is decreased. The effect has been replicated experimentally several times (DeSilva and Bartley, 1930; Fry and Bartley, 1933), with some focusing primarily on brightness averaging or summation (e.g., Ivanoff, 1947). Fechner's Paradox, unlike binocular rivalry (Levelt, 1965a), results in a temporally and spatially stable brightness percept, although there is a gradual adaptation to brightness that occurs on a slow time scale. The early experiments were done without control for each individual eye's pupil size. Subsequent experiments with artificial pupils verified that the effect was not an artifact of differing pupillary conditions (Levelt, 1965a). Contrast sensitivity is also subject to a similar paradox of binocular combination (Gilchrist and McIver, 1985). Reducing the luminance to one eye lowers binocular contrast sensitivity to a level below that for either eye alone.

Many models have described how monocular signals are combined (Table 1). Models of binocular brightness perception tried to replicate data on Fechner's Paradox (Levelt, 1965a). Other models investigated the superiority of binocular over monocular viewing in detection and discrimination tasks. We have created a taxonomy of three different types of models, those based on weighting the inputs to each eye individually (eye-weighting models), those based on vector summation, and those that are neural network, or at least, neurally inspired models. Table 1 lists all the models we have encountered in the literature. Different models can fit different pieces of data. Some can fit more data but need to change model parameters to fit each data curve. The present development of the FACADE model simulates data on binocular brightness summation and Fechner's Paradox with a single set of parameters, including isobrightness curves (Anstis and Ho, 1998; Levelt, 1965a), the absence of Fechner's Paradox for ganzfeld displays (Bolanowski, 1987; Bolanowski and Doty, 1987; Bourassa and Rule, 1994), and the effect of monocular and binocular contours on binocular brightness in static and flashed displays (Cogan, 1982; Levelt, 1965b).

Table 1

2. Binocular Brightness Data and Simulations

This section summarizes the isobrightness curve data of Levelt (1965a) and Anstis and Ho (1998), then data showing that brightness averaging does not occur for ganzfelds (Bolanowski, 1987; Bourassa and

Rule, 1994), and finally data showing how contours affect binocular brightness perception, in particular how monocular and binocular contours affect flashed monocular stimuli (Cogan, 1982). Model simulations of these data are also shown. Section 3 provides an intuitive explanation of the data. Section 4 highlights key mechanisms used in these explanations. The full model is mathematically defined in the Appendix. Section 5 provides a comparative analysis of other models in the literature.

2.1 Isobrightness Curves

The isobrightness curves of Levelt (1965a) provided a classical demonstration of Fechner's paradox. The curves in Figure 1a join points of equal binocular brightness that were determined by matching or magnitude estimates when the subject viewed a dichoptic display wherein one eye viewed a circular patch of fixed luminance and the other eye viewed a similar patch of variable luminance both of which were binocularly fused. Where the curve folds back in on itself is representative of Fechner's Paradox. Levelt did not, however, examine a broad range of luminances. Anstis and Ho (1998) performed this experiment (Figure 1b) and found that isobrightness curves change shape for higher luminances. For low binocular brightness levels, the isobrightness curves are convex upward; for slightly higher brightnesses they become more linear; and for still higher brightnesses they become concave upward. The FACADE model simulates the changing shape of the isobrightness curves without any change of parameters (Figure 1c), unlike the vector summation model of Curtis and Rule (1978), whose isobrightness curves do not change shape (Figure 1d). Binocular brightness model outputs are often compared with the Curtis and Rule model (Lehky, 1983); however, without a continuous change of parameters, the vector sum motion model cannot fit the Anstis and Ho (1998) data.

Figure 1

Another way to view these data shows how, for a fixed luminance signal to one eye, binocular brightness magnitude estimates vary with the luminance to the other eye. The resulting curve has a U-shape (Figure 2a). Figure 2b shows the equivalent output of the FACADE model.

Figure 2

2.2 Binocular Summation of Ganzfeld Brightnesses

In the presence of dichoptically viewed ganzfelds, Fechner's paradox does not occur (Bolanowski, 1987; Bourassa and Rule, 1994). In particular, as one fixes the ganzfeld luminance to one eye and varies the luminance of the other ganzfeld, binocular brightness increases (Figure 3).

Figure 3

Our explanation of binocular brightness summation under these conditions uses the property that positive model activity occurs in response to homogeneous areas of luminance. This hypothesis is compatible with data of Knau and Spillmann (1997), as well as with other data and models (Arend, 1973; Grossberg and Wyse, 1991; Neumann, 1993; Pessoa *et al.*, 1995), which show that, following adaptation to ganzfelds, the remaining perceived brightness is still above that of the *Eigengrau* (Aubert, 1865) — a nonzero brightness associated with a completely dark scene. The model simulations shown in Figure 3 fit these binocular brightness summation data using the same parameters that fit the Fechner’s Paradox data in Figures 1 and 2. For details about how model outputs were scaled to match the magnitude estimations, see Section 4.2.

2.3 Contour Effects on Binocular Brightness

The ganzfeld results suggest that, in the absence of contours, brightness signals summate. Leibowitz and Walker (1956) demonstrated that as the size of two square fields, viewed dichoptically, increases from 15 to 60 min in width, brightness summation (measured by a brightness-matching procedure) triples. They noted that, as field size increases, area increases more rapidly than border length. They suggested that homogeneous areas tend to produce binocular brightness summation, but that boundary contours inhibit the summation process.

Levelt (1965b) showed that when two black disks are fused together, the percept is of a black disk (see Figure 4 disk B). When a black disk is “fused” with a homogeneous white area, the binocular percept is of a dark disk (Figure 4 disk C). However, if a black disk is fused with a circular white area bounded by a thin black contour, one sees a lighter gray disk (Figure 4 disk A). Levelt inferred that the addition of contours biases the binocular brightness percept to the eye containing the contour, thus allowing the binocular disk to appear light gray.

Figure 4

Cogan (1982) examined how various dichoptically viewed backgrounds affect detection sensitivity for monocular flashes of light. Cogan investigated several backgrounds (see Figure 5): (a) homogeneous fields in both eyes; (b) thin circular contour in non-test eye; (c) thin circular contours in both eyes; (d) homogeneous background in test eye, black disk in non-test eye; and (e) thin circular contour in test eye, black disk to non-test eye. The contour exactly spanned the size of the test flash, which was always to the left eye (LE).

Cogan reported the results of six subjects and their respective sensitivities to the conditions (see Figure 6a). The bars represent average subject sensitivities, and the error bars represent the standard deviation of the average across subjects. Across all subjects, flash sensitivity was highest for condition (a) with two homogeneous background fields. For conditions (b) and (c), sensitivity was approximately equal showing that (1) contours reduce sensitivity to the flash, and that (2) there is very little, if any, sensitivity difference between a monocular and binocularly viewed contour. Conditions (d) and (e) have high inter-subject variability possibly due to the rivalrous conditions created by the flash (LE) and black disk (RE) in condition (d) or outline contour (LE) and the black disk contour (RE) in condition (e).

Figure 5

Our model simulations are shown in Figure 6b. The simulations agree with the Cogan (1982) data for conditions (a), (b) and (c) showing increased flash sensitivity on a homogeneous background and the similarity between conditions (b) and (c). Results for condition (d) is slightly different from that recorded by Cogan but still within the bounds of the error bars. The model's sensitivity for condition (e), however, is greater than that recorded by Cogan's subjects. We suggest that the reason for this slight difference may be due to the presence of binocular rivalry in these conditions, which may have partially disrupted the binocular brightness percept and reduced subject sensitivities to the flash in Figure 6a. We do not model binocular rivalry here, but it has been modeled as part of FACADE theory in a manner that is consistent with our results (Grossberg, 1987).

Figure 6

3. Intuitive Explanations of Binocular Brightness Data

3.1 From Discounting the Illuminant to Binocular Surface Brightness

FACADE theory traces properties of binocular brightness data to the combined effects of several basic neural processes. These processes discount the illuminant and binocularly combine the illuminant-discounted signals. The binocular signals then trigger diffusive filling-in of surface representations that carry perceived properties of form, color (including lightness and brightness), and depth (Grossberg, 1994, 1997; Grossberg and McLoughlin, 1997). The present modeling work also clarifies how the nonlinear signaling that occurs during these processes impacts percepts of binocular brightness.

Figure 7

Figure 7 presents a macrocircuit of the FACADE model. The model consists of two parallel systems called the Boundary Contour System (BCS) for binocular boundary formation and the Feature Contour System (FCS) for binocular surface formation. The BCS models aspects of the interblob cortical processing stream and the FCS models aspects of the cortical blob stream from the lateral geniculate nucleus (LGN) to extrastriate visual area V4 (Grossberg, 1994). The FCS boxes that are outlined with dashed lines in Figure 7 are not simulated here because their main effects occur in percepts where multiple depths are seen.

The left-eye and right-eye Monocular Preprocessing stages in Figure 7 model a key process in the retina and LGN; namely, the process of discounting the illuminant (Helmholtz, 1962). Discounting the illuminant helps the brain to compensate for variable illumination conditions. This first stage of the discounting process occurs before signals from the two eyes are combined binocularly. It can be neurally realized using networks of cells whose inputs are processed by on-center off-surround spatial interactions, and which obey the membrane, or shunting, equations of neurophysiology (Grossberg, 1973, 1983). In an on-center off-surround network, the inputs excite their target cells and perhaps close neighbors of these cells, and inhibit a broader spatial expanse of neighboring cells. If the on-center and off-surround are perfectly balanced, then spatially uniform input intensities are completely suppressed. If the on-center has a net advantage over the off-surround, then spatially uniform input intensities can cause an attenuated, but positive, baseline of activity.

The network's ability to discount the illuminant derives from how its shunting dynamics interact with its on-center off-surround interactions. The shunting property enables each cell in the network to automatically gain control its responses to inputs. Cell response rates and equilibrium values are both influenced by this automatic gain control property. In particular, such a network generates its largest activations at edges of a scene, or any other scenic regions where the spatial gradient of input intensity changes quickly relative to the size of the off-surrounds. These enhanced activities discount the illuminant because they include ratio terms (see Section 3.5 and the Appendix) in which the illuminant gets divided out by cancellation in the numerator and the denominator. The enhanced activities that occur at image gradients are called Feature Contours, because they are the signals from which visible surface "features" are derived.

Said more technically, the automatic gain control of a shunting cell computes a Weber-law modulated measure of surface reflectance relative to an adaptation level (Grossberg, 1983; Grossberg and Todorović, 1988). By creating these ratios, the network also tends to normalize image intensities, and thus to compute normalized contrasts from the image, a property that has been used to explain many psychophysical and neurophysiological data (e.g., Douglas *et al.*, 1995; Grossberg, 1973; Grossberg and Marshall, 1989;

Grossberg and Mingolla, 1985a, 1985b; Grossberg and Todorović, 1988; Heeger, 1992; Somers *et al.*, 1995). For present purposes, this fact is relevant to the early realization of Fry and Bartley (1933) that image contrast, and not luminance, influence binocular brightness perception during Fechner's Paradox.

3.2 Surface Filling-In Within Boundary Contours

As noted above, discounting the illuminant distorts the input pattern by attenuating monocular inputs over surface regions that receive uniform, or close-to-uniform, input intensities. This is the price paid for being able to generate relatively large Feature Contour signals from which the illuminant is discounted. These distortions are followed by a process of surface reconstruction whereby features of lightness, brightness, and color are restored throughout a surface, not just near its edges and other contours. Filling-in accomplishes this reconstruction process by using the illuminant-discounted Feature Contour signals to trigger a diffusive spread of activation across the discounted surface areas (Arrington, 1994; Cohen and Grossberg, 1984; Grossberg and Todorović, 1988; Pessoa *et al.*, 1995). In particular, Arrington (1994) has shown that the temporal dynamics of the diffusion process that was modeled in Grossberg and Todorović (1988) can simulate subject reports of the temporal dynamics of perceived surface brightness (Paradiso and Nakayama, 1991).

The diffusion of activation cannot be allowed to spread indiscriminately. Boundary Contours block, or gate, the diffusion of activity in a form-sensitive fashion. Both Boundary Contours and Feature Contours are needed because they compute quite different properties in order to do their jobs well. In fact, FACADE theory has emphasized that the properties of boundary formation and of surface filling-in are, in many respects, computationally *complementary*. For example, Boundary Contour System (BCS) boundaries form in an *oriented* fashion and do so *inwardly* across space between pairs or greater numbers of similarly oriented and spatially aligned boundary inducers. They also pool responses at each position from cells that are sensitive to opposite contrast polarities; in this sense, they become *insensitive* to contrast polarity. This property enables boundaries to form around objects whose contrasts with respect to their backgrounds reverse along the object's perimeter, as often happens when the background that bounds an object is textured. Such a pooling of dark/light and light/dark signals prevents boundaries from representing any visible feature, such as a brightness or color. In this sense, "all boundaries are invisible".

Only surfaces represent visible features. The surface filling-in process is complementary to the boundary formation process because spreads *outwardly* in an *unoriented* fashion from individual Feature Contours, and is *sensitive* to contrast polarity, since it represents visible percepts. Hence, our study of binocular brightness percepts necessarily focuses on the binocular representation of surface brightness. It

involves boundary formation only insofar as Boundary Contours control which surfaces fill-in and what their resultant activity levels are.

These binocular brightness percepts are computed at the processing stage called the Binocular Filling-In Domains, or FIDOs, in Figure 7. Figure 7 also shows other places where filling-in occurs; namely, the Monocular FIDOs. The Monocular FIDOs do not play a major role in explaining many binocular brightness percepts, such as those studied here, that are perceived at a single depth plane. That is why they are not used in our data simulations. Monocular FIDOs are, however, critical in explanations of data that involve multiple depth planes and figure-ground percepts such as percepts of occluding and occluded figures; see Grossberg (1994, 1997) for examples.

3.3 Computation of Binocular Boundaries and Surfaces

The present model also omits the BCS stage in Figure 7 that is called Binocular Boundaries. This is the stage at which boundaries are *completed* across regions that get no bottom-up boundary signals; e.g., the parts of illusory contours that get no bottom-up inputs, or the parts of boundaries that group across spatially separated texture elements. In the present examples, all of the images have complete edges, so the boundaries get direct bottom-up inputs from all input positions. Only the Binocular Fusion stage of the BCS is needed to form simple boundaries of this type. This stage brings together inputs from both eyes to start forming binocular boundaries at positions that do receive bottom-up inputs. In particular, the Left Monocular Boundary and Right Monocular Boundary stages contain simple cells, whose oriented receptive fields detect oriented contrasts in the images. The Binocular Fusion stage contains complex cells, which pool inputs from pairs of simple cells that are sensitive to the same orientation but opposite contrast polarities. In response to the experimental displays that are simulated herein, these complex cells create boundaries that are good enough to restrict, or gate, the binocular surface filling-in process within the appropriate image regions.

The signals that trigger filling-in at the Binocular FIDOs are derived by binocularly combining the illuminant-discounted output signals from the left-eye and right-eye Monocular Preprocessing stages. The cells at which this binocular combination occurs obey the same type of shunting dynamics in an on-center off-surround network that was used at the Monocular Preprocessing stages. Thus, the same types of cells and cell connection patterns operate at every stage of the model's surface processing. As a result, the binocular network also contrast-normalizes its inputs, which in this case are sums of signals from the two eyes. This is the main reason in the model why closing one eye does not make the world look half as bright. This property was also noted by Cohen and Grossberg (1984).

Further properties are needed to explain how brightness can appear to decrease when an input is added to one eye while holding the input to the other eye fixed. Here we need to consider the signal functions that transform the activities of the Monocular Preprocessing stages into inputs to the Binocular FIDO. In particular, we need to specify the excitatory inputs that are processed by the on-center and the inhibitory signals that are processed by the off-surround of the binocular combination network. Earlier mathematical analyses of such networks have clarified why the brain often uses a sigmoid, or S-shaped, excitatory signal function to activate the on-center (Cohen and Grossberg, 1983; Grossberg, 1973, 1983). Such a signal function can help to suppress noise at low input levels, but necessarily has a finite upper bound at high input levels, because all biological signals do; see signal function $f(x)$ in Figure 8a. If the inhibitory signal function $g(x)$ in the off-surround grows more quickly than the excitatory signal function at low input levels, then it can also help to prevent noise amplification.

Figure 8

3.4 Coupling Nonlinear Signals to Shunting Cell Dynamics

One finer feature needs to be mentioned about the dynamics of membrane, or shunting, equations and how they interact with the nonlinear S-shaped signals $f(x)$ and $g(x)$ in Figure 8a. Cells that obey a membrane equation have finite maximum and minimum activities beyond which they cannot be driven by inputs, no matter how large those inputs might be. Such cells also have a resting level to which their activity converges in the absence of input stimulation. We scale this resting level to equal zero herein, without a loss of generality. It is often the case that cells can be maximally excited to activities that are further from their resting levels than the levels to which they can be maximally inhibited. Parameters B and D in Figure 8b represent these asymmetrically chosen excitatory and inhibitory saturation values. Figure 8b shows how these shunting parameters multiply the signal functions $f(x)$ and $g(x)$ in the binocular shunting equation. Terms $Bf(x)$ and $Dg(x)$ preserve the noise-suppressing advantage of inhibition at small input values, but also give a net advantage to excitation at large input values. This combination of noise-suppressing and excitatory signalling properties will be seen to be critical in our explanations of binocular brightness data. We will hereby link paradoxical properties like Fechner's Paradox to functionally useful properties like contrast-normalization and noise-suppression of binocularly combined Feature Contour signals.

These properties are enough to intuitively understand how the FACADE model explains quite a few binocular brightness data. The reader can skip to Section 4 for such explanations. The remainder of this section mathematically defines the binocular shunting equation that is the basis for the key model properties. The Appendix provides the full set of FACADE equations and parameters that were used in the data simulations.

3.5 Equation for Binocular Combination of Feature Contours

Let y_i be the activity of the i^{th} cell in the network that binocularly combines output signals from the Monocular Preprocessing Stages. Then y_i obeys the shunting on-center off-surround equation:

$$\frac{dy_i}{dt} = -\alpha_1 y_i + (B + y_i) \sum_{k=1}^n C_{ki} x_k^+ - (y_i + D) \sum_{k=1}^n E_{ki} x_k^- \quad , \quad (1)$$

In (1), $\frac{dy_i}{dt}$ is the rate of change of y_i ; α_1 is the decay rate; B, D are the upper and lower bounds of activity, or saturating potentials; and C_{ki} and E_{ki} are space-dependent kernels with C_{ki} the excitatory on-center Gaussian kernel and E_{ki} the inhibitory off-surround Gaussian kernel. The excitatory input in (3) is x_k^+ and the inhibitory input is x_k^- . As a result of binocular matching, x_k^+ is a sum of left-eye $f(x_{kL})$ and right-eye $f(x_{kR})$ signals:

$$x_k^+ = f(x_{kL}) + f(x_{kR}); \quad (2)$$

So is the inhibitory input x_k^- :

$$x_k^- = g(x_{kL}) + g(x_{kR}). \quad (3)$$

Taken together, (1) – (3) imply:

$$\frac{dy_i}{dt} = -\alpha_1 y_i + (B + y_i) \sum_{k=1}^n C_{ki} [f(x_{kL}) + f(x_{kR})] - (y_i + D) \sum_{k=1}^n E_{ki} [g(x_{kL}) + g(x_{kR})], \quad (4)$$

where the excitatory signal function $f(x)$ and the inhibitory signal function $g(x)$ are defined as follows:

$$f(x) = \frac{[x - \Gamma]^+2}{\alpha_2^2 + [x - \Gamma]^+2} \quad , \quad (5)$$

$$g(x) = \frac{[x - \Gamma]^+}{\alpha_2 + [x - \Gamma]^+} \quad , \quad (6)$$

and $[x]^+ = \max(x, 0)$ is a half-wave rectifying function. These functions are plotted in Figure 8a. Lehky (1983) suggested a similar asymmetry between excitation and inhibition; however, there are significant differences between the models that are discussed below.

At equilibrium, $\frac{dy_i}{dt} = 0$ in (4) and

$$y_i = \frac{B \sum_{k=1}^n C_{ki}[f(x_{kL}) + f(x_{kR})] - D \sum_{k=1}^n E_{ki}[g(x_{kL}) + g(x_{kR})]}{\alpha_2 + \sum_{k=1}^n C_{ki}[f(x_{kL}) + f(x_{kR})] + \sum_{k=1}^n E_{ki}[g(x_{kL}) + g(x_{kR})]}. \quad (7)$$

The ratio in (7) discounts the illuminant and contrast-normalizes the binocular inputs. As in Figure 8b, the inhibitory saturation point D in (7) is chosen smaller than the excitatory saturation point B . The resting equilibrium potential equals zero. These parameter choices are consistent with known properties of neurons, since the resting membrane potential (-60 to -70 mV) is typically closer to the inhibitory saturation point (-70 to -80 mV) than to the excitatory saturation point (+55 mV) (Kandel, Schwartz and Jessell, 1991). Since both signal functions f and g in (9) have the same asymptote (see Figure 8a), we can choose the parameters ($B = 1.5$, $D = 1.0$) so that the excitatory influence can outweigh the inhibitory influence at small input levels, but the reverse holds true at large input levels (see Figure 8b).

The binocular signals y_i then activate filling-in within the Binocular FIDO (Figure 7). The diffusing activities spread until they are stopped by boundary signals from the BCS, thereby creating the visible binocular surface representation of the model.

4. Intuitive Data Explanations

4.1 Intuitive Explanation of Fechner's Paradox

The relative growth rates of the excitatory and inhibitory signals help to explain binocular brightness summation and Fechner's Paradox in a unified way. At high luminance levels, binocular summation occurs since, in that operating range, the excitatory signal is larger than the corresponding inhibitory signal (Figure 8a). Thus increases in luminance to either eye lead to increases in cell excitation that exceed increases in cell inhibition, thereby causing increased binocular brightness.

However, given a fixed, moderately-sized monocular input, say to the left eye, then increasing the luminance of the right eye input leads to Fechner's Paradox: Since the left eye input is fixed, its effect on binocular brightness is also fixed. As the right eye input is increased from zero, initially its inhibitory signal is greater than its excitatory signal. Therefore the right-eye input causes a greater increase in inhibition than excitation, thereby decreasing the overall binocular output. For ever larger right-eye inputs, the brightness decrement decreases as the excitatory signal eventually outweighs the inhibitory signal, thereby exhibiting binocular brightness summation once more.

4.2 Intuitive Explanation of Brightness Summation for Ganzfelds

The excitatory and inhibitory signals $f(x)$ and $g(x)$ multiply on-center and off-surround connection weights C and E , respectively, in (7) in addition to the excitatory and inhibitory cell saturation values B and D . How these triple products $BCf(x)$ and $DEg(x)$ are combined determines other important data properties, including binocular brightness summation of ganzfeld inputs.

As noted in Section 2.2, a net positive response to homogeneous areas of luminance can help to explain data on binocular summation in response to ganzfelds. One way to realize this luminance response is to employ asymmetric Gaussian receptive fields to define the on-center and off-surround connections C and E in (7). This geometric asymmetry in on-center off-surround connection strengths C and E is consistent with the asymmetry in excitatory and inhibitory saturation values B and D . Given these parameter choices, the on-center signal is stronger than the off-surround signal, so network activity can increase in response to increasing luminance within homogeneous areas. Several studies in monkey and cat primary visual cortex, often using different anesthetics to those used previously, or even using alert animals, showed “luxotonic” cells that respond to such contour-less ganzfeld fields in proportion to the luminance of that field (Barlow and Levick, 1969; Kayama *et al.*, 1979).

This net advantage of the on-center was implemented for both monocular and binocular center-surround cells, so that the luminance response propagated through all the network’s processing stages. At low luminances, the asymmetry has little effect on the network’s contrast-based responses. However, at high luminances, the network’s luminance-based responses can overtake its contrast-based responses. Network responses to ganzfelds are almost entirely luminance-based responses.

After these signals fill-in their surface representation, the filled-in binocular outputs were scaled to match the magnitude estimations of Bourassa and Rule (1994) using the following equation, where B is the binocular brightness output of the network:

$$\text{Magnitude} = 241 \times (B - 0.094). \quad (8)$$

The results are plotted in Figure 3. It should be noted that ganzfelds are featureless and the boundary that traps the filled-in brightness signal is created by the rapid fall-off in luminance near the ganzfeld’s peripheral edge.

4.3 Intuitive explanation of the Cogan (1982) Data

The network responds to ganzfelds with little response at low luminances and larger responses at higher luminances. In response to images that do have contours within them, the network can respond more vigorously to contrastive regions than to homogenous regions. Thus near a contour, the monocular

and binocular brightness signals are dominated by the signal given by the contrastive contour. It is assumed that the binocular network responses activate output pathways which contain transmitter substances that gate, or multiply, the outputs before they activate subsequent processing stages. These transmitters habituate in response to the output signals in their pathways. Such habituating transmitter gates have been used to explain many types of visual data (e.g., Abbott *et al.*, 1997; Francis and Grossberg, 1996a, 1996b; Grossberg, 1980, 1987, 1997; Ögmen and Gagné, 1990). The transmitter-gated responses approximate the formula:

$$S = \frac{After}{\alpha + Before} - \Gamma, \quad (9)$$

where *Before* and *After* are the filled-in binocular brightnesses before and after the flash, α is a constant ($\alpha = 0.001$), and Γ is a threshold parameter ($\Gamma = 0.5$). The *Before* term acts like a Weber-law term that modulates sensitivity to the *After* term. The parameters α and Γ were chosen to fit the detection sensitivities of psychophysical observers in the Cogan (1982) experiment.

The model S values for each condition are given in Figure 6b. For a homogeneous background, the activity before the flash is very low, so even a low luminance flash is detectable. When the before-flash condition includes contrastive monocular or binocular contours, a greater before-flash activity obtains. Increases in the *Before* value decrease the sensitivity of S to the *After* value. Since the flashes are often coextensive with the disk and outline contours, lateral inhibition via off-surround connection between contour and flash signals can reduce the sensitivity to these flashes still further. Thus the same off-surround signals that play a role in explaining Fechner's Paradox are also predicted to play a role in explaining how contours influence binocular brightness percepts.

5. Discussion

The FACADE model of binocular brightness perception uses a single choice of parameters to simulate Fechner's Paradox, brightness summation for ganzfelds, and influences of monocular and binocular contours on binocular brightness percepts. The Fechner's Paradox isobrightness curves reported in Figure 1b are derived from the binocular fusion of light target disks on a dark background. Anstis and Ho (1998) also reported data on the binocular fusion of dark spots on a lighter background. They reported isobrightness curves that do not exhibit the fold-back indicative of Fechner's Paradox. Nor do these data curves change shape as markedly when target disk luminance is varied. We propose that the difference between these datasets may derive from the subjective difficulty in determining an object's brightness when it is placed on a brighter background as opposed to a darker background. Subjects typically find it easier to match for brightness (i.e. "light intensity") when the fused and comparison disks are on a black back-

ground and for lightness (i.e. “grayness”) when the disks are darker than the surround. Thus we suggest that when the background was lighter, subjects may have been matching based on lightness and not brightness. Thus properties of lightness constancy may help explain the lack of change in the shape of the curves. In this paper we focus on explaining data on perceived intensity or luminance — i.e. brightness — and not on lightness (Gilchrist, 1994). Similar models have, however, been used to explain challenging data on the perception of lightness (Grossberg, 1983; Kelly and Grossberg, 1998).

The following sections compare the FACADE model to several other models that have attempted to explain the types of data simulated herein; see Table I.

5.1 Models of Binocular Brightness and Fechner’s Paradox

Three types of models have previously been proposed to explain data on binocular brightness and contrast combination. *Eye-weighting models* date back to Sherrington (1908) and Schrödinger (1926). Their monocular weights often depend on the amount of contour or contrast presented to each eye. *Vector summation models* binocularly sum two monocular vectors. *Neural network or neurally-inspired models* typically incorporate excitatory and inhibitory mechanisms. Fry and Bartley (1933) were perhaps the first to suggest a neural basis for Fechner’s Paradox. They proposed excitatory and inhibitory processes such that binocular brightness is more brilliant than either monocular impression when binocular neural excitation more than compensates for inhibition. To help readers understand some of the capabilities of the models discussed, Figures 9 and 10 show the isobrightness curves for each model with a fixed parameter set.

Figures 9 and 10

5.1.1 Eye-weighting Models

Levelt (1965) Weighted Sum Model. In this influential model, Levelt computed binocular brightness as follows:

$$C = W_L E_L + W_R E_R , \tag{10}$$

where C is the binocular brightness, E_L and E_R are the luminances of the fused left- and right-eye targets, and W_L and W_R are weighting coefficients that, in general, reflect the amount of contour in each eye’s image, with the constraint that $W_L + W_R = 1$. This model is only capable of averaging the two inputs and cannot model binocular brightness summation, since C can never be greater than E_L or E_R due to the restriction on the weights. The model also lacks a computational rule to allow the choice of weights. Figure 10a shows isobrightness curves for parameters $W_L = W_R = 0.5$. Unlike the psychophysical data on Fech-

ner's Paradox, the isobrightness lines do not curve out or in and, most importantly, do not wrap back in at the ends, as shown in Levelt (1965a) and Anstis and Ho (1998).

Engel (1969) Autocorrelation Model. Here binocular brightness equals:

$$C = \sqrt{(W_L B_L)^2 + (W_R B_R)^2}, \quad (11)$$

with weights such that $W_L^2 + W_R^2 = 1$. Quantity C can be interpreted as the sum of two orthogonal vectors. Quantities B_L and B_R are monocular brightness signals, not luminances, since Fry and Bartley (1933) and Teller and Galanter (1967) showed that contrast, and not luminance *per se*, affect binocular brightness. To convert from brightness to luminance, it is assumed that brightness is related to luminance by a power function with exponent $k=0.33$. Then equation (10) can be expressed using monocular luminances E_L and E_R :

$$C = \sqrt{(W_L E_L^k)^2 + (W_R E_R^k)^2}, \quad (12)$$

This model also includes a restriction on the weights that does not allow for binocular summation. However, unlike the Levelt (1965a, 1965b) model, the weighting coefficients in the Engel (1969) model can be determined by finding the integral of the squared autocorrelation function for the pattern in each eye. The resulting number measures the amount of contour and contrast in that eye.

To fit the data, however, Engel (1970) had to make assumptions about the inputs; e.g., nonzero brightness is associated with a black background like the "eigenraum" (Aubert, 1865). Engel (1970) also reinterpreted the evidence for binocular summation in Fry and Bartley (1933) by suggesting an influence of the comparison target contours on the test target brightness. He concluded erroneously that binocular summation does not occur and that the experimental results are artifactual. Despite discussion of weightings for ganzfeld inputs (Engel, 1967), the restriction that the weights sum to 1 does not allow the model to replicate binocular brightness summation data. Figure 9b shows the isobrightness curves of this model for $W_L^2 = W_R^2 = 0.5$. The isobrightness curves are convex, and lack the wrap-in at the curve ends.

de Weert and Levelt (1974) Centroid Model. de Weert and Levelt suggested the following model:

$$C = \frac{W_L (E_L + a)^{2n} + W_R (E_R + a)^{2n}}{W_L (E_L + a)^n + W_R (E_R + a)^n}, \quad (13)$$

where C is the binocular output, W_L , W_R are “eye dominance factors” such that $W_L + W_R = 1$, and E_L and E_R are monocular luminance signals. Quantity a is a small positive constant that is assumed to be associated with stray light, and n is an exponent for a power function with value between 0.3 and 0.4. In this model, the quantitative differences between the values of C are very small. Decreases of binocular brightness are at most 3.7% for Fechner’s Paradox, whereas for summation, there is just a 0.8% increase (Curtis and Rule, 1978). These relative magnitudes do not agree with observed magnitude estimation and brightness match differences (Bourassa and Rule, 1994; Curtis and Rule, 1980; Levelt, 1965a). Figure 9c shows the isobrightness curves displayed by this model with $a=0.0001$, $n = 0.33$. These curves do curve outward somewhat and also wrap back in at the ends, however the shape of the curves remain constant, unlike the Anstis and Ho (1998) data.

Irtel’s (1986) Model. Irtel also proposes another weighted-eye model:

$$C = w_L g(E_L) + w_R g(E_R), \quad (14)$$

where E_L and E_R are the monocular signals. Once again, $W_L + W_R = 1$, since:

$$W_L = \frac{g(E_L)}{g(E_L) + g(E_R)} \quad (15)$$

Using $g(a) = a^\beta$, equations (15) and (16) imply:

$$C = \frac{E_L^{2\beta} + E_R^{2\beta}}{E_L^\beta + E_R^\beta}. \quad (16)$$

Irtel (1986) suggested varying β for differing left- and right-eye luminances, but like Levelt, did not suggest a computational rule. Irtel’s model can model the different shape isobrightness curves for certain values of β ($0 < \beta < 0.5$). However, Irtel (1986) does not explain how the model might operate if the stimuli are ganzfelds of disparate luminance, nor does it include mechanisms by which monocular contours might affect binocular brightness. Figure 9d shows the isobrightness curves for $\beta=0.33$. The curves exhibit the wrap-in and are slightly convex, but their shape is the same regardless of luminance.

5.1.2 Vector Summation models

Schrödinger (1926) and MacLeod (1972) Model. Schrödinger (1926) suggested that binocular brightness perception is not a result of simple addition of monocular signals. Instead he proposed the following model:

$$B = E_L \left(\frac{E_L}{E_L + E_R} \right) + E_R \left(\frac{E_R}{E_L + E_R} \right)$$

$$= \frac{E_L^2 + E_R^2}{E_L + E_R}, \quad (17)$$

where E_L and E_R are monocular “brightness flux” signals and the binocular result B can be viewed as the sum of two orthogonal vectors with some normalization. B is interpreted as the “length” of the two monocular brightness “vectors”. The model is quite similar to that of Irtel (1986), which it predated by 60 years. MacLeod (1972) modified this model to preprocess the input:

$$E_L = \begin{cases} E_0 + \log \frac{\phi_L}{\phi_0} & \text{if } \phi_L \geq \phi_0 \\ E_0 & \text{if } \phi_L < \phi_0 \end{cases}, \quad (18)$$

Here the left eye input, E_L , is a function of spontaneous activity E_0 and the difference ϕ_L in luminance across a monocular contour, normalized by the threshold luminance difference, ϕ_0 . The monocular right eye input E_R is defined similarly. This preprocessing represents approximately logarithmic processing by retinal ganglion cells. It allows the isobrightness curves to wrap back in at the ends, as in Figure 10e with $\phi_0=0.05$ and $E_0=0.1$, but the shape of the curve remains unchanged at higher total luminances.

Curtis and Rule (1978) Vector Summation Model. Engel (1967) was one of the first to propose a vector summation model, but he postulated that the vectors (i.e., the monocular input signals) being summed were orthogonal. In response to problems with the relative magnitudes of the de Weert and Levelt (1974) Centroid model, Curtis and Rule (1978) proposed a vector summation model to combine the two eye’s monocular brightness inputs B_L , B_R :

$$C = \sqrt{B_L^2 + B_R^2 + 2(B_L B_R \cos \alpha)}. \quad (19)$$

To convert from brightnesses to luminances we use a power law:

$$C = \sqrt{E_L^{2k} + E_R^{2k} + 2(E_L^k E_R^k \cos \alpha)}, \quad (20)$$

Parameter k is set as before to 0.33. For α in the range 90 to 120 degrees, Fechner’s Paradox is observed (i.e., the curves wrap back in on themselves). Figure 9f shows the isobrightness curve output of the model

with $\alpha = 120^\circ$. Although α relates to the amount of contour in an image, Curtis and Rule (1978) do not describe a computational rule for how α may be calculated, and they cannot model how the different isobrightness curve shapes arise without a change of parameters. Cohn, Leong and Lasley (1981) also used this model to explain binocular discrimination data and to argue for the presence of two channels, one that sums monocular signals and another that calculates their difference.

Legge (1984) Quadratic Summation Model. Legge (1984) presented a rule describing binocular contrast summation to explain data on contrast detection, contrast discrimination, dichoptic masking, contrast matching and reaction-time data:

$$C = \sqrt{C_L^2 + C_R^2}. \quad (21)$$

Here C_L and C_R are the left- and right-eye contrasts. Although Legge (1984) used this model to simulate several aspects of binocular over monocular performance, he did not simulate Fechner's paradox. Increasing a target's contrast with the background increases that target's brightness, thus (21) can be used to estimate how monocular luminances combine. In fact, the model cannot simulate Fechner's Paradox because its two monocular signals summate and generate circular isobrightness curves (Figure 10a).

5.1.3 Neural Network Models

Sugie's (1982) Inhibitory Threshold Model. As in the FACADE model, Sugie uses excitatory and inhibitory interactions, but they are between the monocular channels, not within the binocular summation equations, as they are in the FACADE model. Sugie achieves Fechner's Paradox using neural thresholds and asymmetric excitation and inhibition. The left- and right-eye inputs for the binocular equation are as follows:

$$N_L = f(E_L - h_R E_R) \quad (22)$$

and

$$N_R = f(E_R - h_L E_L), \quad (23)$$

where E_L and E_R are monocular luminance signals, and h_L and h_R control the inhibitory signals, or "threshold characteristics", of the neurons. Sugie set $h_L = h_R$, and $f(x) = \max(x, 0)$. Terms N_L and N_R are the responses of cells receiving strong excitation to one eye and weak inhibition from the other eye. These responses are binocularly combined as follows:

$$C = N_L + N_R. \quad (24)$$

Fechner's Paradox is explained since, when one monocular luminance is low and the other is high, the mutual inhibition causes a reduction in overall output. Brightness summation data cannot be simulated, since interocular inhibition has the same relative magnitude for large and small inputs. By setting such inhibition to zero these data could be modeled, but that would represent a different observer. Figure 10b shows the isobrightness curve outputs by Sugie's model with $h_L = h_R = 0.25$.

Lehky (1983) Nonlinear Summation Model. The model that is most similar to how the FACADE model combines monocular brightness signals is that of Lehky, who assumed different signal functions for the excitatory and inhibitory terms of his equation such that the inhibition initially outgrows the linear excitation. By using a compressive nonlinearity, the inhibitory signal function initially outgrows the linear excitation function, but later the excitatory influences dominate. As with Sugie, Lehky first calculated monocular signals N_L and N_R :

$$N_L = E_L \left[1.0 - m \left(\frac{N_R}{N_L + N_R} \right)^n \right] \quad (25)$$

and

$$N_R = E_R \left[1.0 - m \left(\frac{N_L}{N_L + N_R} \right)^n \right], \quad (26)$$

where $m > 0$, $0 < n < 1$, and $E_L, E_R \geq 0$. Functions E_L and E_R are the "firing rates of peripheral inputs" and involve logarithmic processing of the inputs (see below). Parameter m controls the relative strength of inhibition between the two eyes. Parameter n determines the compressive nonlinear inhibition ($n=0.69$). The inputs were calculated much as in the MacLeod (1972) model of equation (18), namely:

$$E_L = k \ln \left(\frac{I_L}{I_T} \right), \quad (27)$$

and similarly for E_R . Term I_L is the "stimulus intensity", presumably luminance, and I_T is a threshold. Initially, $N_L = E_L$ and $N_R = E_R$. The equations were iterated until the change in N_L and N_R was less than 0.00001. Binocular output was calculated as follows:

$$C = N_L + N_R. \quad (28)$$

Lehky (1983) simulated the isobrightness curve of Levelt (1965b). Figure 10c shows how the model simulates Fechner's Paradox and the data of Anstis and Ho (1998). His model can also simulate contour effects by increasing the parameter m on the side with the contour and decreasing m for the other side. Then the side with the contour more strongly inhibits the non-contour side and dominates the network out-

put. However, the model does not code for any spatial interactions and thus cannot explain data on how monocular and binocular contours affect binocular brightness perception (Cogan, 1982) without a change in parameters. More generally, no internal mechanism is identified with which to justify these stimulus-dependent parameter changes.

Cogan (1987) Two Channel Model: Two channel models use separate monocular and binocular channels. The Cogan (1987) model is formally equivalent to a vector summation model:

$$C = \frac{E_L}{1 + cE_R} + \frac{E_R}{1 + cE_L} + kE_LE_R, \quad (29)$$

where E_L and E_R are left-eye and right-eye inputs and $c > 0$, and $k \geq 0$ are parameters. By dividing each monocular signal by the opposite eye signal, Cogan realized a form of shunting inhibition. Cogan (1987) did not discuss how his model might explain the absence of Fechner's Paradox for ganzfelds, nor how the presence of contours affects brightness perception.

Figure 10d shows the output of the Cogan model for $c=1.0$ and $k = 0.1$. These parameters are different than those given by Cogan because they better fit data of Anstis and Ho (1998), as well as Fechner's Paradox. Although the FACADE model predicts the same qualitative isobrightness curves, our models are testably different. Cogan uses shunting inhibition and multiplicative excitation to binocularly combine his left- and right-eye inputs. FACADE uses addition of nonlinear signals to binocularly combine both excitation and inhibition within a single shunting equation, with no monocular interocular inhibition.

Gregson (1989) Nonlinear Model. Gregson proposed a complex recursive nonlinear equation that exhibits quite complicated nonlinear dynamics which we will not describe here. Gregson's (1989) model predicts the shape of the isobrightness curve data for higher and lower luminances than Levelt's (1965a, 1965b) data. This predicted curve differs from data of Levelt (1965a) and Anstis and Ho (1998). See Figure 11a. The curves do not display Fechner's Paradox. They do change shape for higher combined luminance levels, but do not display the convex shape of the Anstis and Ho (1998) data at low luminances.

Anderson and Movshon (1989) Distribution Model: This model possesses several linear binocular channels. Each channel has a degree of ocular dominance wherein each channel is more or less sensitive to each eye; i.e., some cells are more sensitive to left-eye inputs, others to right-eye inputs, and others are balanced. The authors also suggest that these channels may be thresholds and only channels with suprathreshold activity influence the binocular result. Thus for various interocular contrast differences, a different pattern of activity will exist across this distributed binocular channel representation. Anderson and Movshon (1989) suggested that the envelope of these channels traces a contour resembling that for threshold

detection data; see Figure 11b. If it is assumed that binocular brightness is a similar function of that envelope, then the model cannot explain the Levelt (1965a) or Anstis and Ho (1998) data.

Figure 11

5.2 Some Neurophysiological Correlates

The FACADE model uses nonlinear excitatory and inhibitory signal functions coupled to shunting equations that exhibit automatic gain control, adaptation, and saturation effects. Nonlinear responses in cortical cells that exhibit automatic gain control, adaptation and saturation effects are well documented in the literature (see Pinter and Nabet, 1992 for a review). See Ferster (1994) for a review of evidence for nonlinear synaptic interactions in cat cortical cells. Kayama *et al.* (1979) noted that two-thirds of cells in monkey striate cortex cells that respond to ganzfeld stimuli are binocular and many exhibited complex binocular interactions. Anzai, Barse, Freeman and Cai (1995) found evidence for nonlinearities in the contrast response function of binocular simple and complex cells of area 17 of anesthetized and paralyzed adult cats similar to the excitatory function $f(x)$ in Figure 8a. Anzai *et al.* (1995) also suggested that the presence of an adaptive threshold mechanism in these cells, similar to the nonlinear inhibitory signal function $g(x)$. Bonds (1992) provided evidence that, similar to our binocular FCS cells, the excitatory and inhibitory bandpasses (i.e., signal functions) of simple cells in cat striate differed quite clearly in their shape and that this difference varied with contrast. Bonds (1992) suggests that the orientation bias of a simple cell could be refined if “the threshold mechanism could adapt to different stimulus contrasts, yielding a slight amount of threshold at low contrasts and proportionally more at higher contrasts”. These data pertain to cells that correspond to the Boundary Contour System of our model. We predict that similar properties will be seen in binocular cells corresponding to the model Feature Contour System which calculates surface brightness; i.e., binocular cells that are color-selective and possibly lacking strong orientation selectivity. These cells probably exist in visual areas beyond primary visual cortex, such as areas V2 or V4 in monkey visual cortex (Desimone *et al.*, 1985; Zeki, 1983a, 1983b) where it has been suggested the binocular surface representations of FACADE exist (Grossberg, 1994).

One physiological correlate of Fechner’s Paradox could be suppression of monocular responses in binocular cells. Berardi *et al.* (1986) found evidence for suppression in binocular neurons of cat visual cortex. In particular, if a high and low contrast grating were presented simultaneously, one to each eye, then the binocular cell’s response to the low contrast stimulus was suppressed. Sengpiel *et al.* (1994) and Smith *et al.* (1997) have shown similar suppression in binocular complex and simple cells of monkey visual cortex.

Based on visual evoked potentials (VEP), Denny, *et al.* (1991) suggested that binocular cells could be influenced by tonic inhibition from either eye. This tonic inhibition may increase the relative inhibitory influence over these cells at low activations and may be one source of the signal function asymmetries. Denny *et al.* (1991) presented evidence that the effect of this tonic inhibition is most visible when one eye is dark adapted, leading to increased sensitivity in the other eye, much as in the data of Buck and Pulos (1987), who observed interaction between rods of one eye and cones in the other eye. Zemon *et al.* (1993) used VEP recordings to suggest that monocular signals are combined in a nonlinear fashion. They used their data to argue against the models of Curtis and Rule (1978), Legge (1984), and Anderson and Movshon (1989).

Bibliography

- Abbott, L.F., Varela, K., Sen, K., & Nelson, S.B. (1997). Synaptic depression and cortical gain control. *Science*, 275, 220-223.
- Anderson, P.A. & Movshon, J.A. (1989) Binocular combination of contrast signals. *Vision Research*, 29, 1111-1132.
- Anstis, S. & Ho, A. (1998) Nonlinear combination of luminance excursions during flicker, simultaneous contrast, afterimages and binocular fusion. *Vision Research*, 38, 523-539.
- Anzai, A., Bearnse, M. A., Freeman, R.D., & Cai, D. (1995) Contrast coding by cells in the cat's striate cortex: Monocular vs. Binocular Detection. *Visual Neuroscience*, 12, 77-93.
- Arend, L. (1973) Spatial differential and integral operations in human vision: Implication of stabilized retinal image fading. *Psychological Review*, 80, 374-395.
- Arrington, K.F. (1994) The temporal dynamics of brightness filling-in. *Vision Research*, 34, 3371-3387.
- Aubert, H. (1865) *Physiologie der Netzhaut*. Breslau: Morgenstern.
- Barlow, H. & Levick, W. (1969) Changes in maintained discharge with adaptation level in the cat retina. *Journal of Physiology, London*, 202, 699-718.
- Berardi, N., Galli, L., Maffei, L., & Siliprandi, R. (1986) Binocular suppression in cortical neurons. *Experimental Brain Research*, 63, 581-584.
- Blake, R. & Fox, R. (1973) The psychophysical inquiry into binocular summation. *Perception and Psychophysics*, 14, 161-185.
- Blake, R., Sloane, M., & Fox, R. (1981) Further developments in binocular summation. *Perception and Psychophysics*, 30, 266-276.
- Bolanowski, S.J. (1987) Contourless stimuli produce binocular summation. *Vision Research*, 27, 1943-1951.
- Bolanowski, S.J. & Doty, R.W. (1987) Perceptual "blankout" of monocular homogeneous fields (Ganzfelder) is prevented with binocular viewing. *Vision Research*, 27, 967-982.
- Bonds, A.B. (1992) Spatial and temporal nonlinearities in receptive fields of the cat striate cortex. In Pinter, R.B. & Nabet, B. (Eds.) *Nonlinear vision: Determination of neural receptive fields, function, and networks* (pp. 329-352). Boca Raton, FL: CRC Press
- Bourassa, C.M. & Rule, S.J. (1994) Binocular brightness: A suppression-summation trade off. *Canadian Journal of Experimental Psychology*, 48, 418-433.

- Buck, S.L. & Pulos, E. (1987) Rod-cone interaction in monocular but not binocular pathways. *Vision Research*, 27, 479-482.
- Cogan, A.I. (1982) Monocular sensitivity during binocular viewing. *Vision Research*, 22, 1-16.
- Cogan, A.I. (1987) Human binocular interaction: Towards a neural model. *Vision Research*, 27, 2125-2139.
- Cohen, M.A. & Grossberg, S. (1983). Absolute stability of global pattern formation and parallel memory storage by competitive neural networks. *IEEE Transactions on Systems, Man, and Cybernetics*, 13, 815-826.
- Cohen, M.A. & Grossberg, S. (1984) Neural dynamics of brightness perception: Features, boundaries, diffusion, and resonance. *Perception and Psychophysics*, 36, 428-456.
- Cohn, T.E., Leong, H., & Lasley, D.J. (1981) Binocular luminance detection: Availability of more than one central interaction. *Vision Research*, 21, 1017-1023.
- Curtis, D.W. & Rule, S.J. (1978) Binocular processing of brightness information: A vector-sum model. *Journal of Experimental Psychology: Human Perception and Performance*, 4, 132-143.
- Curtis, D.W. & Rule, S.J. (1980) Fechner's paradox reflects a nonmonotone relation between binocular brightness and luminance. *Perception and Psychophysics*, 27, 263-266.
- Denny, N., Frumkes, T.E., Barris, M.C. & Eysteinson, T. (1991) Tonic interocular suppression and binocular summation in human vision. *Journal of Physiology*, 437, 449-460.
- DeSilva, H.R. & Bartley, S.H. (1930) Summation and subtraction of brightness in binocular perception. *British Journal of Psychology*, 20, 242-252.
- Desimone, R., Schein, S.J., Moran, J., & Ungerleider, L.G. (1985) Contour, color, and shape analysis beyond the striate cortex. *Vision Research*, 25, 441-452.
- de Weert, C.M.M. & Levelt, W.J.M. (1974) Binocular brightness combinations: Additive and nonadditive aspects. *Perception and Psychophysics*, 15, 551-562.
- Douglas, R.J., Koch, C., Mahowald, M., Martin, K.A.C., and Suarez, H.H. (1995). Recurrent excitation in neocortical cells. *Science*, 269, 980-985.
- Engel, G.R. (1967) The visual processes underlying binocular brightness summation. *Vision Research*, 7, 753-767.
- Engel, G.R. (1969) The autocorrelation function and binocular brightness mixing. *Vision Research*, 9, 1111-1130.
- Engel, G.R. (1970) Tests of a model of binocular brightness. *Canadian Journal of Psychology*, 24, 335-352.

- Fechner, G.T. (1861) Über einige verhältnisse des binocularen Sehens. *Abh. sachs. Ges. (Akad.) Wiss.*, 7, 337-564.
- Ferster, D. (1994) Linearity of synaptic interactions in the assembly of receptive fields in cat visual cortex. *Current Opinion in Neurobiology*, 4, 563-568.
- Francis, G. and Grossberg, S. (1996a). Cortical dynamics of form and motion integration: Persistence, apparent motion, and illusory contours. *Vision Research*, 36, 149-173.
- Francis, G. and Grossberg, S. (1996b). Cortical dynamics of boundary segmentation and reset: Persistence, afterimages, and residual traces. *Perception*, 25, 543-567.
- Fry, G.A. & Bartley, S.H. (1933) The brilliance of an object seen binocularly. *American Journal of Ophthalmology*, 16, 687-693.
- Gilchrist, A. (Ed.) (1994) *Lightness, Brightness and Transparency*. Hillsdale, NJ: Lawrence Erlbaum Associates.
- Gilchrist, J. & McIver, C. (1985) Fechner's paradox in binocular contrast sensitivity. *Vision Research*, 25, 609-613.
- Gove, A., Grossberg, S., & Mingolla, E. (1995) Brightness perception, illusory contours and cortico-geniculate feedback. *Visual Neuroscience*, 12, 1027-1052.
- Gregson, R.A.M. (1989) A nonlinear systems approach to Fechner's Paradox. *Biological Cybernetics*, 61, 129-138.
- Grossberg, S. (1973) Contour enhancement, short-term memory, and constancies in reverberating neural networks. *Studies in Applied Mathematics*, 52, 217-257.
- Grossberg, S. (1980) How does the brain build a cognitive code? *Psychological Review*, 87, 1-51.
- Grossberg, S. (1983) The quantized geometry of visual space: The coherent computation of depth, form and lightness. *The Behavioral and Brain Sciences*, 6, 625-692.
- Grossberg, S. (1987) Cortical dynamics of three-dimensional form, color and brightness perception: II. Binocular Theory. *Perception and Psychophysics*, 41, 117-158.
- Grossberg, S. (1994) 3-D Vision and figure-ground separation by visual cortex. *Perception and Psychophysics*, 55, 48-120.
- Grossberg, S. (1997) Cortical dynamics of three-dimensional figure-ground perception of two-dimensional pictures. *Psychological Review*, 104, 618-658.
- Grossberg, S. & Marshall, J. A. (1989) Stereo boundary fusion by cortical complex cells: A system of maps, filters, and feedback networks for multiplexing distributed data. *Neural Networks*, 2, 29-51.

- Grossberg, S. & McLoughlin, N.P. (1997) Cortical dynamics of three-dimensional surface perception: Binocular and half-occluded scenic images. *Neural Networks*, 10, 1583-1605.
- Grossberg, S. & Mingolla, E. (1985a) Neural dynamics of form perception: Boundary completion, illusory figures, and neon color spreading. *Psychological Review*, 92, 173-211.
- Grossberg, S. & Mingolla, E. (1985b) Neural dynamics of perceptual grouping: Textures, boundaries and emergent features. *Perception and Psychophysics*, 38, 141-171.
- Grossberg, S. & Todorović, D. (1988) Neural dynamics of 1-D and 2-D brightness perception: A unified model of classical and recent phenomena. *Perception and Psychophysics*, 43, 241-277.
- Grossberg, S. & Wyse, L. (1991) A neural network architecture for figure-ground separation of connected scenic figures. *Neural Networks*, 4, 723-742.
- Hamada, J. (1984) A multi-stage model for border contrast. *Biological Cybernetics*, 51, 65-70.
- Heeger, D.J. (1992) Normalization of cell responses in cat striate cortex. *Visual Neuroscience*, 9, 181-197.
- Helmholtz, H. von (1962) *Treatise on physiological optics*. J.P.C. Southall (Translation). New York: Dover.
- Hodgkin, A.L. (1964) *The conduction of the nervous impulse*. Springfield: C.C. Thomas.
- Howard, I.P. & Rogers, B.J. (1995) *Binocular Vision and Stereopsis*. Oxford Psychology Series, No. 29. New York: Oxford University press.
- Irtel, H. (1986) Experimente zu Fechners Paradoxon der binokularen Helligkeit. *Zeitschrift für Experimentelle und Angewandte Psychologie*, 33, 413-422.
- Ivanoff, A. (1947) Au sujet de l'expérience de Fechner. *Acad. Sci. Opt. Physiol.*, May 19th, 224, 1443-1455.
- Kandel, E.R., Schwartz, J.H. & Jessell, T.M. (1991) *Principles of Neural Science*, (3rd Edition). New York: Elsevier.
- Kayama, Y., Riso, R., Bartlett, J.R., & Doty, R.W. (1979) Luxotonic responses of units in Macaque Striate cortex. *Journal of Neurophysiology*, 42, 1495-1517.
- Kelly, F.J. & Grossberg, S. (1997) Cortical mechanisms of 3-D pop-out and amodal completion. *ARVO Abstracts, Investigative Ophthalmology & Visual Science*, 38 (4), S969.
- Kelly, F.J. and Grossberg, S. (1998) How does visual cortex determine surface brightness during figure-ground perception. *ARVO abstracts, Investigative Ophthalmology & Visual Science*, 39 (4), S326

- Kingdom, F. & Moulden, B. (1992) A multi-channel approach to brightness coding. *Vision Research*, 32, 1565-1582.
- Knau, H. & Spillmann, L. (1997) Brightness fading during ganzfeld adaptation. *Journal of the Optical Society of America A*, 14, 1213-1222.
- Land, E. & McCann, J. (1971) Lightness and retinex theory. *Journal of the Optical Society of America*, 61, 1-11.
- Legge, G.E. (1984) Binocular contrast summation II. Quadratic summation. *Vision Research*, 24, 385-94.
- Lehky, S.R. (1983) A model of binocular brightness and binaural loudness perception in humans with general applications to nonlinear summation of sensory inputs. *Biological Cybernetics*, 49, 89-97.
- Leibowitz, H. & Walker, L. (1956) Effect of field size and luminance on the binocular summation of Suprathreshold Stimuli. *Journal of the Optical Society of America*, 46, 171-172.
- Levelt, W.J.M. (1965a) *On binocular rivalry*. Institute for Perception Monograph, R.V.O.-T.N.O. Soesterberg, The Netherlands.
- Levelt, W. J. M. (1965b) Binocular brightness averaging and contour information. *British Journal of Psychology*, 56, 1-13.
- MacLeod, D. I. A. (1972) The Schrödinger equation in binocular brightness combination. *Perception*, 1, 321-324.
- McLoughlin, N.P. & Grossberg, S. (1998) Cortical computation of stereo disparity. *Vision Research*, 38, 91-99.
- Neumann, H. (1993) Toward a computational architecture for unified visual contrast and brightness perception: I. Theory and model. In *Proceedings of the World Conference on Neural Networks (WCNN-93)*, Vol. 1, pp. 84-91. Hillsdale, N.J.: Erlbaum.
- Ögmen, H. & Gagné, S. (1990) Neural network architecture for motion perception and elementary motion detection in the fly visual system. *Neural Networks*, 3, 487-506.
- Panum, P.L. (1858) *Physiologische Untersuchungen über das Sehen mitzwei Augen*. Kiel: Schwers.
- Paradiso, M.A. & Nakayama, K. (1991) Brightness perception and filling-in. *Vision Research*, 31, 1221-1236.
- Pessoa, L., Mingolla, E., & Neumann, H. (1995) A contrast- and luminance-driven multiscale network model of brightness perception. *Vision Research*, 35, 2201-2223.

- Pinter, R.B., & Nabet, B. (Eds.) (1992) *Nonlinear vision: Determination of neural receptive fields, function, and networks*. Boca Raton, FL: CRC Press.
- Schrödinger, E. (1926) Die Gesichtsempfindungen. In Mueller-Pouillet's *Lehrbuch der Physik* (11th ed.), Book 2, Part I. Vieweg: Braunschweig, pp.456-560.
- Sengpiel, F., Blakemore, C., Kind, P.C. & Harrad, R. (1994) Interocular suppression in the visual cortex of strabismic cats. *Journal of Neuroscience*, *14*, 6855-6871.
- Sherrington, C.S. (1908) *The integrative action of the nervous system*. London: Constable.
- Smith, E. L., Chino, Y., Ni, J., & Cheng, N. (1997) Binocular combination of contrast signals by striate cortical neurons in the monkey. *Journal of Neurophysiology*, *78*, 366-382.
- Somers, D.C., Nelson, S.B., and Sur, M. (1995). An emergent model of orientation selectivity in cat visual cortical simple cells. *Journal of Neuroscience*, *15*, 5448-5465.
- Sugie, N. (1982) Neural models of brightness perception and retinal rivalry in binocular vision. *Biological Cybernetics*, *43*, 13-21.
- Teller, D.Y. & Galanter, E. (1967) Brightnesses, luminances and Fechner's paradox. *Perception and Psychophysics*, *2*, 297-300.
- Wheatstone, C. (1838) Contributions to the physiology of vision - Part the first. On some remarkable and hitherto unobserved phenomena of binocular vision. *Philosophical Transactions of the Royal Society*, *128*, 371-394.
- White, M. (1979) A new effect of pattern on perceived lightness. *Perception*, *8*, 413-416.
- Zeki, S. (1983a) Colour coding in the cerebral cortex: The reaction of cells in monkey visual cortex to wavelengths and colours. *Neuroscience*, *9*, 741-766.
- Zeki, S. (1983b) Colour coding in the cerebral cortex: The responses of wavelength-selective and colour coded cells in monkey visual cortex to changes in wavelength composition. *Neuroscience*, *9*, 767-791.
- Zemon, V., Pinkhasov, E., & Gordon, J. (1993) Electrophysiological tests of neural models: Evidence for nonlinear binocular interactions in humans. *Proceedings of the National Academy of Sciences USA*, *90*, 2975-2978.

Appendix: Equations and Parameters

This section describes BCS and FCS equations that incorporate the enhancements and revisions discussed in the text. The equations are similar to those in Gove *et al.* (1995) and Grossberg and McLoughlin (1997), but they eliminate processes that are not rate-limiting in the targeted data: Only a single scale is used, and hypercomplex and bipole cells in the BCS and monocular filling-in domains (FIDOs) in the FCS are not included. All equations were solved at equilibrium, except for the binocular filling-in equation which was solved using fourth-order Runge-Kutta with time step 0.0000025. Most of the equations were solved at equilibrium to fit the targeted data. However, as Arrington (1994) and Francis and Grossberg (1996a, 1996b) illustrate, these equations can also be solved in real-time to fit dynamically evolving data.

A1 ON Channel

FACADE cell activities obey the classical membrane equation (Hodgkin 1964; Grossberg 1973, 1983):

$$C_m \frac{dV(t)}{dt} = -[V(t) - E_{excit}]g_{excit}(t) - [V(t) - E_{inhib}]g_{inhib}(t) - [V(t) - E_{leak}]g_{leak}, \quad (A1)$$

where the parameters E represent reversal potentials, g_{leak} is a constant leakage conductance, and the time varying conductances $g_{excit}(t)$ and $g_{inhib}(t)$ represent the total excitatory and inhibitory inputs to the cell. The $V(t)$ terms that multiply these conductances in (A1) represent shunting interactions.

For computational simplicity, the present simulations use only an ON channel. The ON channel activity x_i at each cell i is described by an on-center off-surround network whose cells obey membrane equations:

$$\frac{dx_i}{dt} = -\alpha_1 x_i + (U_1 - x_i) C_i - (x_i + L_i) S_1. \quad (A2)$$

Taken together, the shunting and on-center off-surround interaction in (A2) yield ratio processing and normalization by cell activities x_i (Grossberg, 1973, 1983); *i.e.*, contrast normalization. In (A2) the decay rate $\alpha_1 = 100$; the excitatory and inhibitory saturation levels are $U_1 = 50$ and $L_1 = 50$ respectively; and the center C_1 and surround S_1 terms are defined by Gaussian kernels:

$$C_1 = \sum_p C_p I_{i+p}, \quad (\text{A3})$$

and

$$S_1 = \sum_p S_p I_{i+p}, \quad (\text{A4})$$

with

$$C_p = \frac{A_1}{2\pi\sigma_c^2} \exp\left(-\frac{p^2}{\sigma_c^2}\right), \quad (\text{A5})$$

$$S_p = \frac{A_2}{2\pi\sigma_s^2} \exp\left(-\frac{p^2}{\sigma_s^2}\right), \quad (\text{A6})$$

and $A_1 = 1.1, A_2 = 15.987, \sigma_c = 0.1, \sigma_s = 1.5$. At equilibrium:

$$x_i = \frac{\sum_p (U_1 C_p - L_1 S_p) I_{i+p}}{\alpha_1 + \sum_p (C_p + S_p) I_{i+p}}, \quad (\text{A7})$$

and the output signal $X_i = [x_i]^+$, where $[x]^+ = \max(x, 0)$. The values of A_1 and A_2 were chosen so that a uniform pattern of I_i inputs causes an x_i response pattern whose amplitude is approximately one-tenth as large. This assures a positive response to ganzfelds.

A2 Simple Cells of the BCS

Even-symmetric and odd-symmetric simple cell receptive fields centered on location i were defined using even and odd Gabor kernels. For our 1-D brightness simulations, these terms are:

$$S_i^{odd} = \left[\sum_p s_p^{odd} X_{i-p} \right]^+ \quad (\text{A8})$$

and

$$S_i^{even} = \left[\sum_p s_p^{even} X_{i-p} \right]^+, \quad (\text{A9})$$

where

$$s_p^{odd} = A \sin(2p) \exp\left[-\frac{1}{2} \left(\frac{p^2}{\sigma_p^2}\right)\right] \quad (\text{A10})$$

and

$$s_p^{even} = A \cos(2p) \exp\left[-\frac{1}{2} \left(\frac{p^2}{\sigma_p^2}\right)\right], \quad (\text{A11})$$

$A = 1.0, \sigma_p = 1.0$, and $\sigma_q = 0.75$. The size of the kernel is defined to be $-4 \leq p \leq 4$ in (A8) and (A9).

A3 Complex Cells of the BCS

Complex cell activities c_i fuse together the left and right monocular simple cell boundaries. In this implementation, the two monocular images are at zero disparity:

$$\frac{dc_i}{dt} = -\alpha_3 c_i + (U_3 - c_i) \sum_p C_{i+p} S_{i+p} - (c_i + L_3) \sum_p E_{i+p} S_{i+p}, \quad (\text{A12})$$

where $\alpha_3 = 0.1$, $U_3 = 1.0$, and $L_3 = 1.0$. The term S_{i+p} is the sum of even and odd simple cell activities:

$$S_i = S_i^{\text{even}} + S_i^{\text{odd}}. \quad (\text{A13})$$

The Gaussian on-center and off-surround kernels are:

$$C_{i+p} = A_1 \exp[-\mu^c p^2] \quad (\text{A14})$$

and

$$E_{i+p} = A_2 \exp[-\mu^s p^2], \quad (\text{A15})$$

where $A_1 = 1.0$, $A_2 = 1.0$. $\mu_c = 1.5$ and $\mu_s = 0.06$. At equilibrium:

$$c_i = \frac{\sum_p (U_3 C_{i+p} - L_3 E_{i+p}) S_{i+p}}{\alpha_3 + \sum_p (C_{i+p,d} + E_{i+p,d}) S_{i+p}} \quad (\text{A16})$$

The output from the complex cells is defined as $C_i = [c_i]^+$.

A4 Binocular Filling-In Domain of the FCS

The binocular filling-in domains (FIDOs) receive input from both the left and right eye monocular ON cells. The binocular activities y_i that fuse the left and right eye FCS signals are defined as in (6):

$$\frac{dy_i}{dt} = -\alpha y_i + (B - y_i) \sum_{k=1}^n C_{ki} [f(x_{kL}) + f(x_{kR})] - (y_i + D) \sum_{k=1}^n E_{ki} [g(x_{kL}) + g(x_{kR})], \quad (\text{A17})$$

where C_{ki} and E_{ki} are Gaussian kernels and where the nonlinear signal functions $f(x)$ and $g(x)$ are defined as follows:

$$f(x) = \frac{[x - \Gamma]^+^2}{\alpha + [x - \Gamma]^+^2} \quad (\text{A18})$$

and

$$g(x) = \frac{[x - \Gamma]^+}{\alpha + [x - \Gamma]^+}. \quad (\text{A19})$$

The excitatory function thus grows less quickly than the inhibitory signal function. At equilibrium,

$$y_i = \frac{B \sum_{k=1}^n C_{ki} [f(x_{kL}) + f(x_{kR})] - D \sum_{k=1}^n E_{ki} [g(x_{kL}) + g(x_{kR})]}{\alpha + \sum_{k=1}^n C_{ki} [f(x_{kL}) + f(x_{kR})] + \sum_{k=1}^n E_{ki} [g(x_{kL}) + g(x_{kR})]}. \quad (\text{A20})$$

The output signal is $Y_i = [y_i]^+$. The diffusive filling-in of surface activity Ω_i is defined by the following equations (Grossberg and Todorović, 1988):

$$\frac{d\Omega_i}{dt} = -M\Omega_i + \sum_{p \in N} (\Omega_p - \Omega_i) \Psi_{pi} + Y_i, \quad (\text{A21})$$

where the decay rate $M = 0.1$, $B = 1.5$, $D = 1.0$, N_i is the set of nearest neighbors of cell i , and the permeability coefficient that controls the rate of diffusion is:

$$\Psi_{pi} = \frac{\delta}{\kappa + \epsilon(C_p + C_i)}, \quad (\text{A22})$$

where $\delta = 50,000$, $\kappa = 1.0$, $\epsilon = 50,000$. In (A22), C_p and C_i represent boundary signals at positions p and i that are determined by the complex cell activities at these positions. Solving (A21) at equilibrium yields:

$$\Omega_i = \frac{\sum_{p \in N_i} \Omega_p \Psi_{pi}}{M + \sum_{p \in N_i} \Psi_{pi}}, \quad (\text{A23})$$

A5 Computer Implementation

The computer implementation of the BCS/FCS model is written in C and runs on Sun Workstations. The following sections describe how the equations are used to arrive at the simulation graphs.

A5.1 Isobrightness curves

Because of the computational costs in solving equation (A21) using numerical integration for many points, the isobrightness curve in Figure 1c was generated by varying both left-eye and right-eye inputs and evaluating y_i using equation (A20) at the central binocular FCS cell in the array of 165 cells. The cell's receptive field is nine units wide and (x_{kL}, x_{kR}) were created using equation (A7). The network input I_i corresponds to a single point stimulus presented to both left and right input streams.

The MATLAB contour function was then used to plot the isobrightness curves of y_i values. These curves connect points corresponding to equal binocular FCS filling-in signals. All other things being equal, for a step increase in input luminance, as used in the Anstis and Ho (1998) experiments, larger luminance steps lead to larger filling-in signals which will correspond to larger filled-in values (Grossberg and Todorović, 1988) and so the lines in Figure 1c will connect points of equal filled-in surface brightness signals.

A5.2 U Shape curve

The same functions were used to generate the U shape curve seen in Figure 2b but the left eye input luminance was fixed at 1000 and the right-eye input luminance was varied from 0 to 1000.

A5.3 Ganzfeld Simulations

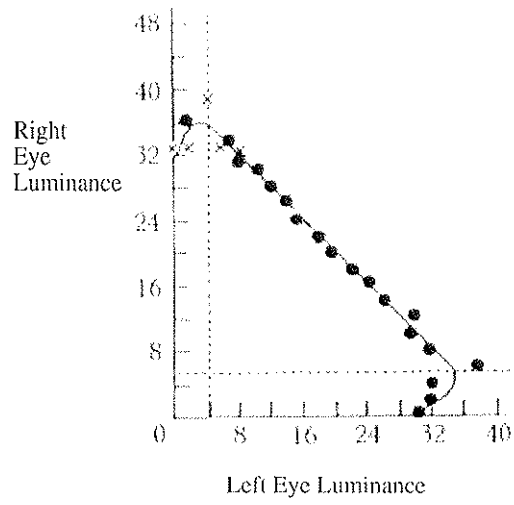
In the ganzfeld simulations, we needed only fit the 12 ganzfeld luminance data points of Bourassa and Rule (1994), so numerical integration of equation (A21) was now tractable. Ganzfeld inputs were created as follows for a 1-D array of 165 cells:

$$I_i = 2\sqrt[3]{(90^2 - (c - i)^2)} + 800, \quad (\text{A24})$$

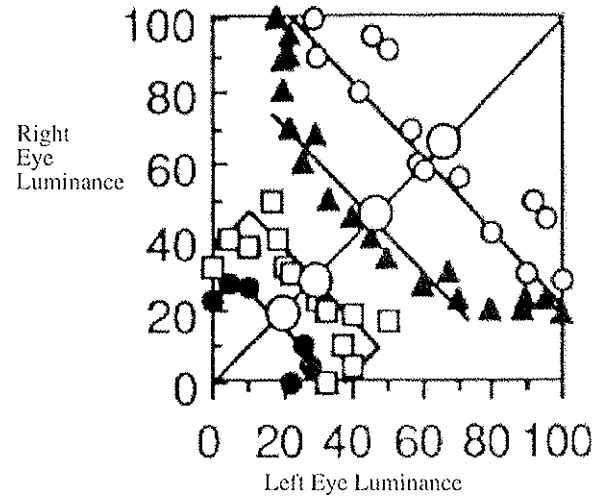
where $c = 83$ is the center node of the network and $i = 1, 2, \dots, 165$. The term $90^2 - (c - i)^2$ generates a smooth 1-D cross section that falls off from the center. The cube root function allows the function fall-off to be less steep with a slightly convex shape. Although Bourassa and Rule (1994) do not discuss the fall-off in luminance at the periphery, typical experimental procedures allow at most a 5% difference between center and periphery (Knau and Spillmann, 1997). The addition of 800 in (A24) defines a base luminance. This luminance cross-section corresponds to the fixed left-eye ganzfeld input. Less luminous right-eye ganzfeld inputs can be created by multiplying each I_i by a scaling factor as dictated by the Bourassa and Rule (1994) luminance values. The final filled-in equilibrium value is scaled using equation (8) in Section 4.2 and plotted beside the average magnitude data from Bourassa and Rule (1994).

A5.4 Cogan data simulations

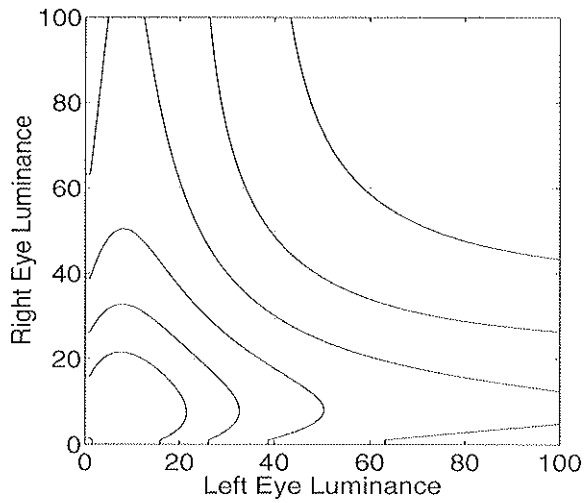
The Cogan inputs were created by using 1-D cross-sections of the left- and right-eye inputs in Figure 5. I_i was set to 0.0 for the black contours and black disk input regions, otherwise I_i was set to 0.6 for the before-flash condition. For inputs containing the flash, I_i was set to 1.0 for those regions that contained the flash, all other inputs are unchanged. Each flash stimulus was 45 cells wide, out of the total 165 cells. The width of the black contour surrounding a flashed stimulus was 4 cells. Model detection sensitivities were modeled by taking the final filled-in binocular FCS signal and applying equation (9) as per Section 4.3.



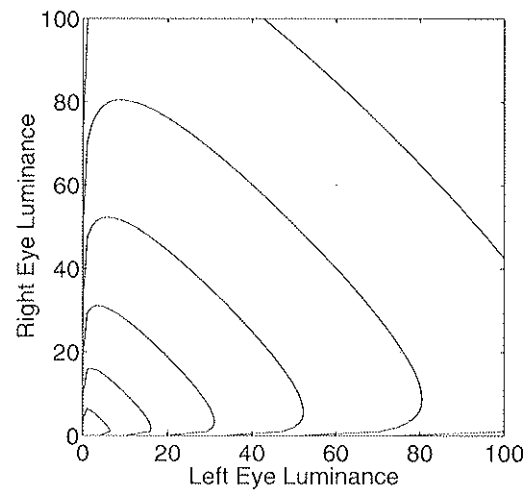
(a)



(b)

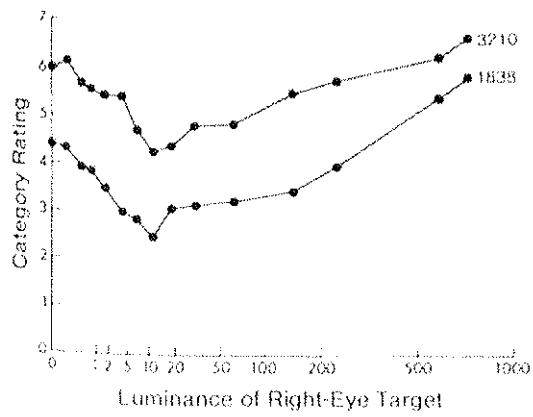


(c)

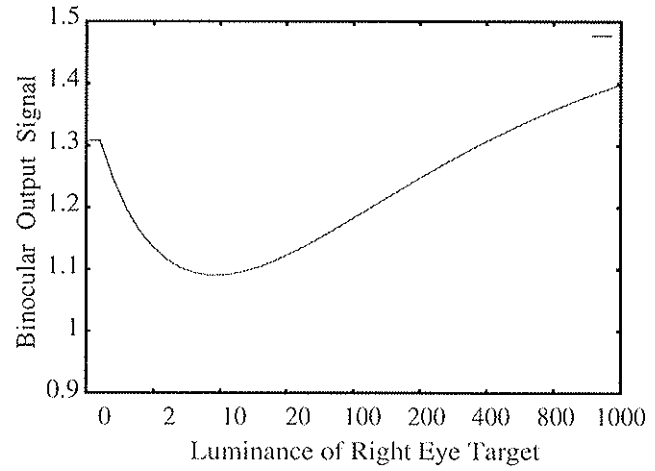


(d)

Figure 1: Isobrightness curves of (a) Levelt (1965) and (b) Anstis and Ho (1998). Reprinted with permission. Isobrightness curves generated by (c) the FACADE model; (d) the vector summation model (Curtis and Rule, 1978).



(a)



(b)

Figure 2: (a) Psychophysical U-shaped data indicative of Fechner's Paradox. Reprinted with Permission from Curtis and Rule (1980). (b) FACADE model simulation.

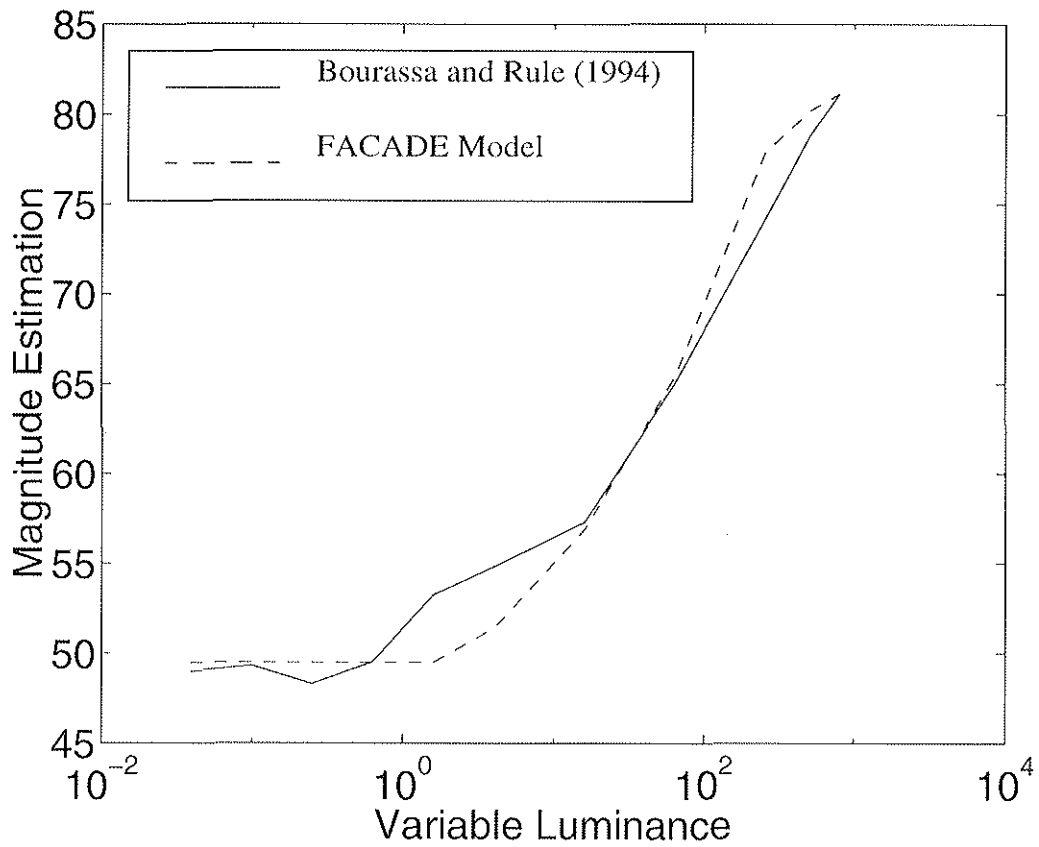


Figure 3: Ganzfeld brightness perception; Data of Bourassa and Rule (1994) and FACADE model simulation. Data are reprinted with permission.

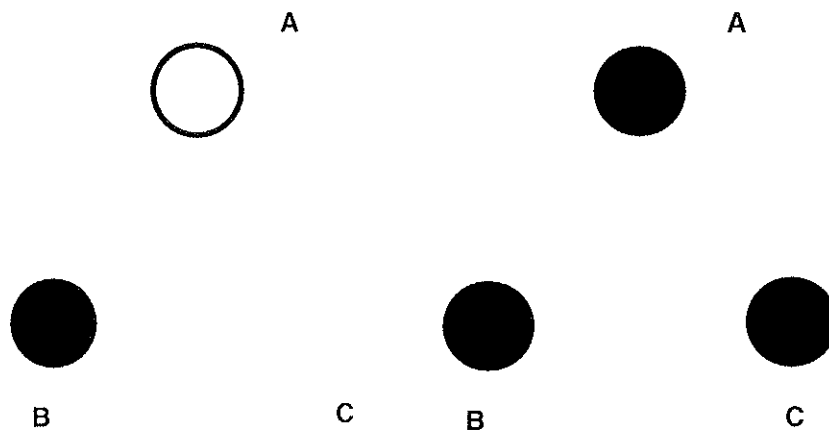


Figure 4: Cross-fusers should be able to fuse three pairs of disks A,B,C (Levelt, 1965b). (A) Fusion of the outline circle with a black disk results in a much brighter percept than (B) fusion of two black disks or (C) the fusion of a homogeneous white area with a black disk. See text for details. Reprinted with permission.

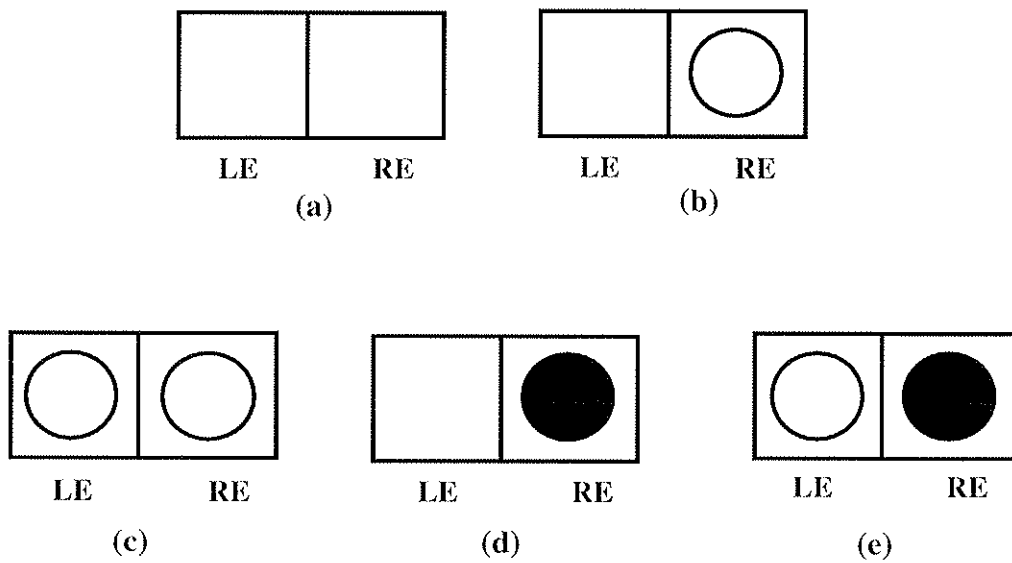
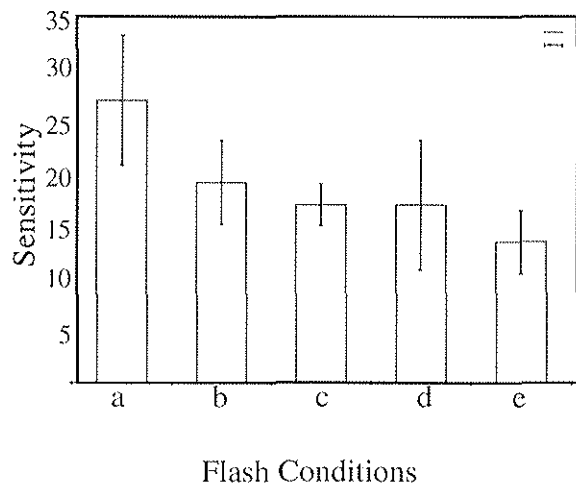
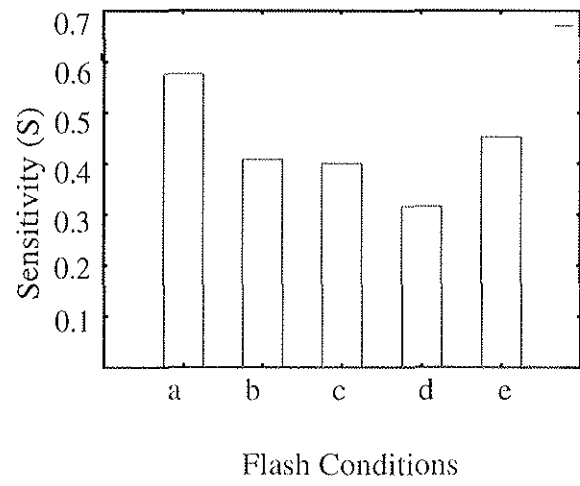


Figure 5: Schematic of left-eye (LE) and right-eye (RE) monocular images seen by viewer before flash to the left eye in the Cogan (1982) study. See text for details. Reprinted with permission.



(a)



(b)

Figure 6: (a) Averaged subject threshold sensitivities (b) FACADE model simulations. See text for details.

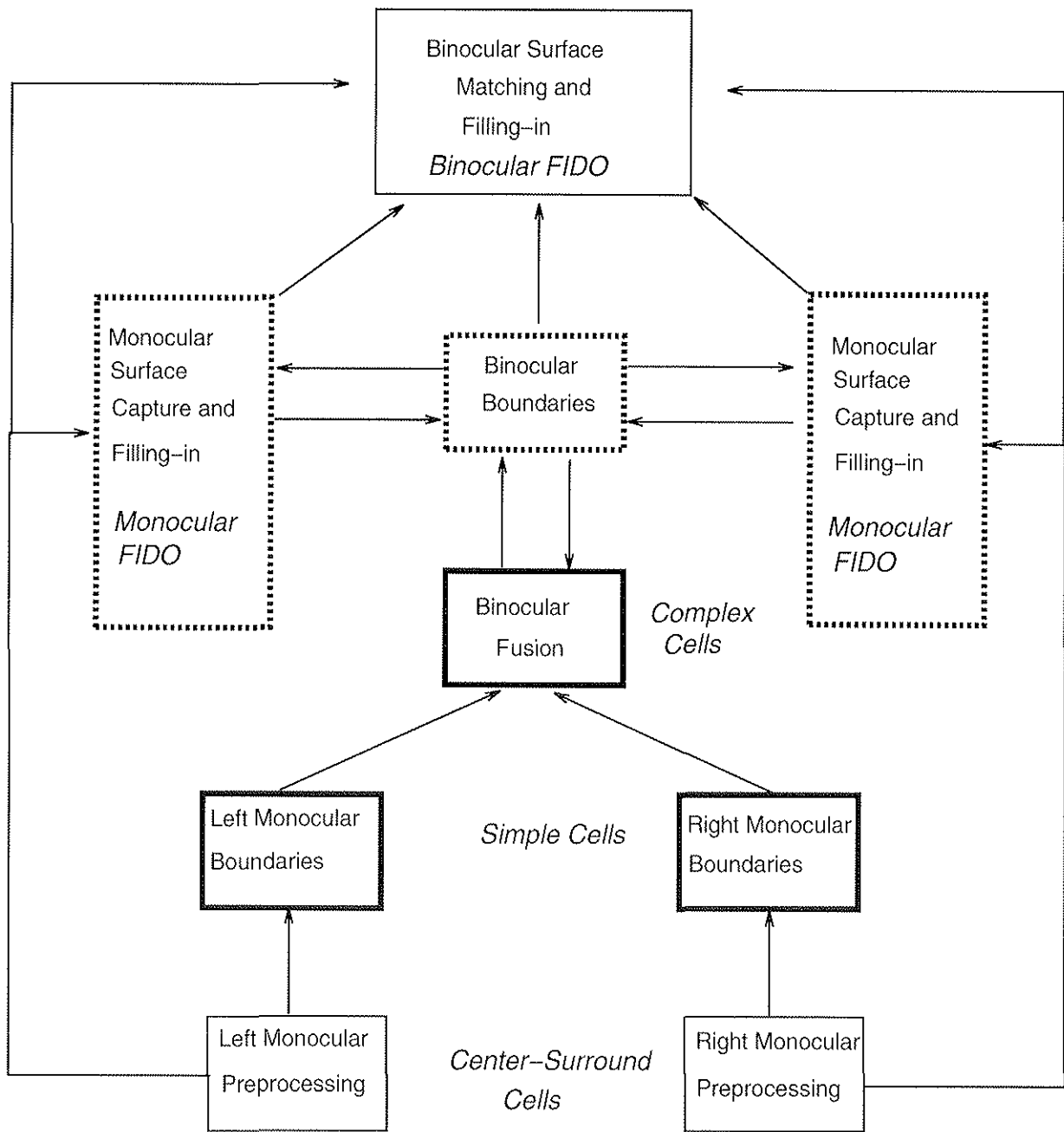


Figure 7: Macrocircuit of FACADE model. Stages surrounded by solid lines represent processes that were simulated in this paper. Dotted lines demarcate processes not simulated here but employed in the simulation of other phenomenon in other FACADE model studies. See text for details.

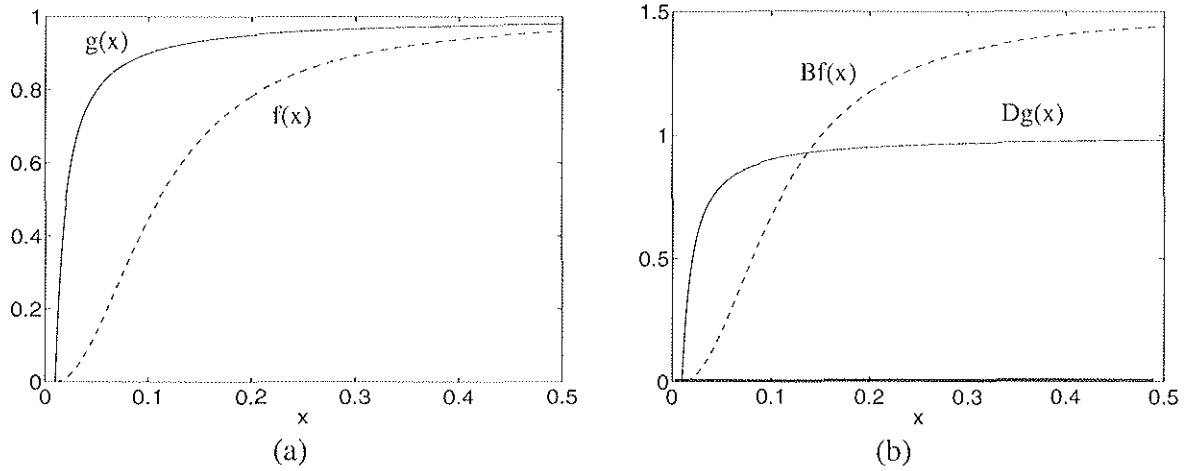


Figure 8: Asymmetric excitatory and inhibitory signal functions, $f(x)$ and $g(x)$, respectively. In (a), $f(x)$ and $g(x)$ asymptote to the same level. In (b), $Bf(x)$ and $Dg(x)$ asymptote to different levels because $B > D$. See text for details about how B and D are chosen.

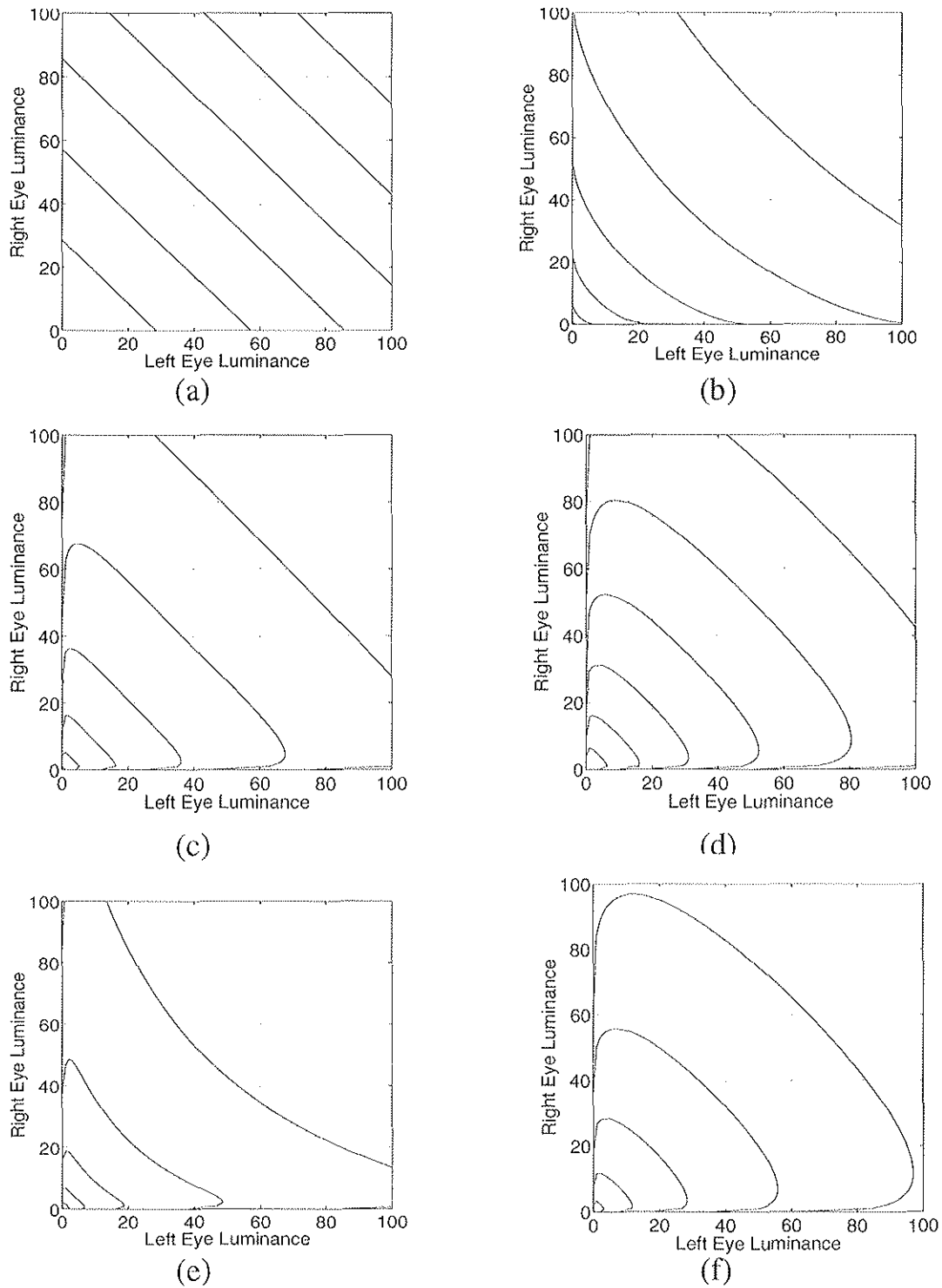
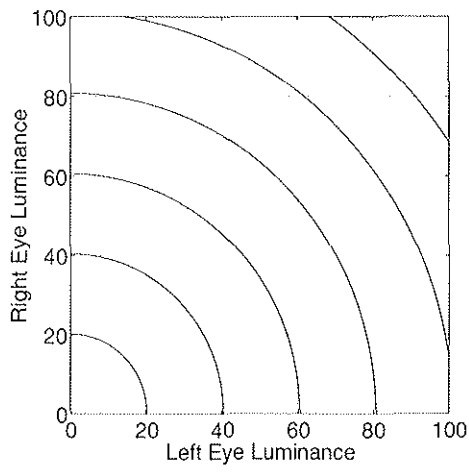
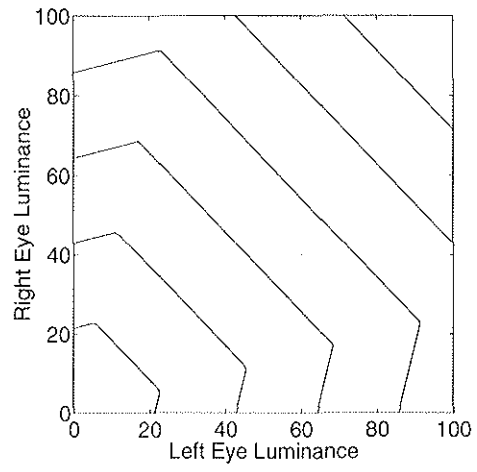


Figure 9: Isobrightness curves for different models (a) Levelt (1965a); (b) Engel (1969); (c) deWeert and Levelt (1974); (d) Irtel (1986); (e) Schrödinger (1926) and MacLeod (1972); (f) Curtis and Rule (1978).

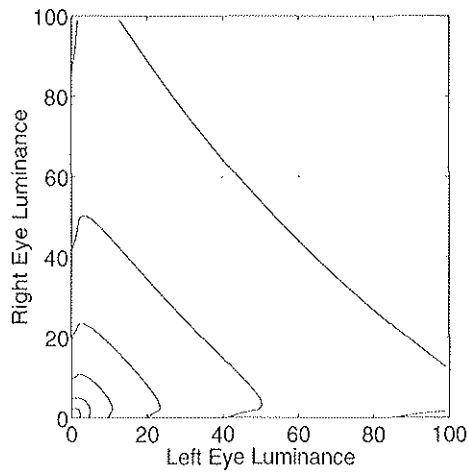
See text for details.



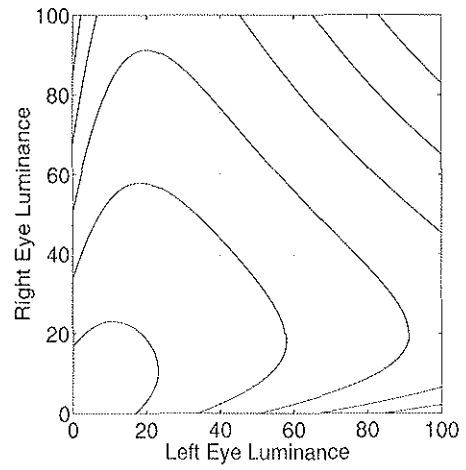
(a)



(b)



(c)



(d)

Figure 10: Isobrightness curves for models by (a) Legge (1984); (b) Sugie (1982); (c) Lehky (1983); (d) Cogan (1987). See text for details.

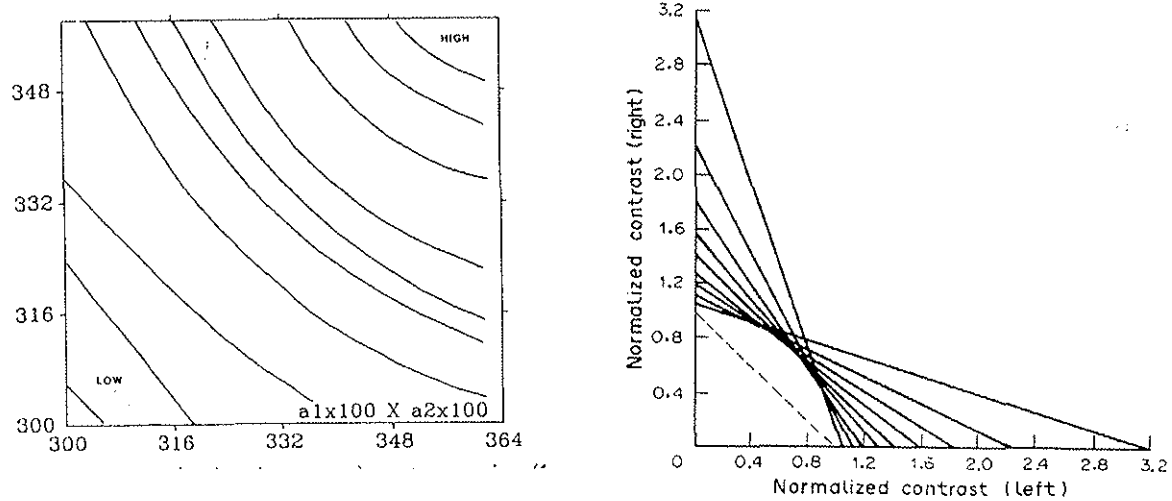


Figure 11: (a) Isobrightness curves predicted by Gregson (1989). Reprinted with permission. (b) Envelope of responses of binocular cells of different ocular dominance of Anderson and Movshon (1989). Reprinted with permission. See text for details.

Author	Model Type	Levelt (1965a,b) Data	Anstis and Ho (1998) Data	Ganzfeld Summation Data	Cogan (1982) Data
Levelt (1965a,b)	Eye-weighting	Yes	No	No	No
Engel (1969)	Eye-weighting	Yes**	No	No	No
de Weert and Levelt (1974)	Eye-weighting	Yes	Yes	No	No
Irtel (1986)	Eye-weighting	Yes	Yes	No	No
Schrödinger / MacLeod (1926/1972)	Vector Summation	Yes	No	No	No
Curtis and Rule (1978)	Vector Summation	Yes	Yes	No	No
Legge (1984)	Vector Summation	Yes	No	No	No
Sugie (1982)	Neural Network	Yes	No	Yes**	No
Lehky (1983)	Neural Network	Yes	Yes	Yes**	No
Cogan (1987)	Neural Network	Yes	Yes	Yes**	No
Anderson and Movshon (1989)	Neural Network	No	No	No	No
Gregson (1989)	Neural Network	Yes	No	No	No
Grossberg and Kelly (1998)	Neural Network	Yes	Yes	Yes	Yes

Table 1: Past models of Binocular Summation and their capabilities

** Yes (with change of parameters).